



Petrogenesis and U–Pb zircon chronology of felsic tuffs interbedded with turbidites (Eastern Pontides Orogenic Belt, NE Turkey): Implications for Mesozoic geodynamic evolution of the eastern Mediterranean region and accumulation rates of turbidite sequences

Yener Eyuboglu*

Karadeniz Technical University, Department of Geology, 61080 Trabzon, Turkey



ARTICLE INFO

Article history:

Received 25 August 2014

Accepted 7 November 2014

Available online 15 November 2014

Keywords:

Zircon chronology

Felsic tuff

Convergent margins

Pull-apart basin

Turbidite

ABSTRACT

The Meso-Cenozoic geodynamic evolution of the Eastern Pontides Orogenic Belt, which is one of the key areas of the Alpine-Himalayan system, is still controversial due to lack of systematic geological, geophysical, geochemical and chronological data. The prevailing interpretation is that this belt represents the southern margin of Eurasia during the Mesozoic and its geodynamic evolution is related to northward subduction of oceanic lithosphere. This paper reports the first detailed geological, geochemical and chronological data from felsic tuffs interbedded with late Cretaceous turbidites in the Southern Zone of the Eastern Pontides Orogenic Belt.

Individual tuff layers are thin, mostly <2 m in thickness, implying that these are dominantly air-fall tuffs. Petrographic data indicate that the felsic tuffs, which exhibit various degrees of alteration, can be classified as crystal-rich and crystal-poor tuffs. The crystal-poor tuffs consist mainly of 45–65% devitrified glass shards and 10–20% broken quartz crystals, whereas the crystal-rich tuffs consist of >50% crystals. The zircon U–Pb data show three statistically distinct ages at 84, 81 and 77 Ma, with uncertainties of about 1 Ma, suggesting that tuff-forming late Cretaceous magmatism started about 84 Ma ago and was episodically active over a minimum of 7 Ma. The age data also indicate that the average accumulation rate of the turbiditic sequence that hosts the felsic tuffs remained constant between 36 and 40 cm/10 ky. Their enrichment in LIL and LRE elements relative to HFS and HRE elements, and also strongly negative Nb, Ta and Ti anomalies, are consistent with those of magmas generated by subduction-related processes. The tuffs have relatively low initial ratios of $^{143}\text{Nd}/^{144}\text{Nd}$ (0.512296–0.512484; ϵ_{Nd} : –2.1 and –7.2) and $^{87}\text{Sr}/^{86}\text{Sr}$ (0.704896–0.706159). Their initial Pb isotopic compositions range from 18.604 to 18.646 for $^{206}\text{Pb}/^{204}\text{Pb}$, from 15.644 to 15.654 for $^{207}\text{Pb}/^{206}\text{Pb}$ and from 38.712 to 38.763 for $^{208}\text{Pb}/^{204}\text{Pb}$. The distribution of Sr–Nd isotopic compositions in the late Cretaceous igneous rocks from different locations of the Eastern Pontides Orogenic Belt is consistent with two-component mixing between depleted mantle and crust. However, the Pb isotopic data are not compatible with two-component mixing and require at least a third component.

Considering all of the new data and also previous data such as southward migration and increasing potassium content of the late Cretaceous arc volcanism, the northward migration of Cenozoic igneous activity, northward drift of the belt since the late Cretaceous and the existence of south-dipping reverse fault systems in the whole region, the Meso-Cenozoic geodynamic evolution of the Eastern Pontides Orogenic Belt can be best explained by southward subduction of Tethys oceanic lithosphere, rather than northward subduction.

© 2014 Elsevier B.V. All rights reserved.

1. Introduction

Convergent plate margins are the sites of most intense geological processes such as magmatism, metamorphism, crust–mantle interaction and related tectonics. Systematic geological, geochemical and chronological studies on the igneous rock groups exposed in fossil convergent margins provide important clues on both conditions required

for the generation of the magmas and the geodynamic evolution of the region. The Eastern Pontides Orogenic Belt represents one of the best examples of a fossil convergent margin in the Alpine-Himalayan belt and its Meso-Cenozoic geodynamic evolution is still controversial due to lack of systematic geological, geochemical and chronological data. In this orogenic belt, Mesozoic time is characterized by three main cycles of igneous activity in the Triassic, the early to middle Jurassic and the late Cretaceous. The Triassic activity is represented mainly by small-scale mafic-ultramafic bodies cutting the basement of the orogenic belt (Eyuboglu et al., 2010, 2011a). Detailed geological,

* Tel.: +90 462 377 2742; fax: +90 462 325 74 05.

E-mail address: yenereyuboglu@gmail.com.

geochemical and isotopic studies clearly indicate that these mafic-ultramafic rocks reveal the geochemical characteristics of subduction-related, high alumina, hydrous basaltic magmas crystallized in small magma chambers at shallow crustal levels (Eyuboglu et al., 2010, 2011a). The early to middle Jurassic igneous activity is mainly represented by basaltic-andesitic volcanic and associated pyroclastic rocks in the Northern Zone of the belt. In the south, the Jurassic magmatism is characterized by felsic lithologies such as granite, granodiorite, dacite and rhyolite and also mafic-intermediate lithologies such as gabbro, diorite, andesite and basalt. There are only a few studies documenting the geochemical characteristics of early to middle Jurassic volcanism in the Eastern Pontides Orogenic Belt. According to Bektaş et al. (1987), the Jurassic volcanism is related to hydrous/anhydrous partial melting of the mantle wedge above southward subducted oceanic lithosphere. Sen (2007) suggested that the Jurassic basaltic-andesitic volcanic rocks were generated by partial melting of metasomatized spinel lherzolite. Most recent systematic geological, geochemical and geochronological studies on Jurassic intrusions in the whole region indicate that subduction-related processes played an important role in their petrogenetic evolution (Eyuboglu, unpublished data). Late Cretaceous time is mainly represented by bimodal volcanic and associated pyroclastic rocks and also granitic intrusions in the Northern Zone of the Eastern Pontides Orogenic Belt. To the south, the intensity of the late Cretaceous igneous activity decreases and clastic sedimentary rocks interbedded with felsic tuffs, which are the main subjects of this study, constitute the dominant lithology.

There is a consensus that the late Cretaceous igneous activity is subduction-related. However, the subduction polarity is still controversial. The main idea is that the Pontides belt was shaped by northward subduction of oceanic lithosphere (Paleotethys or Neotethys) until the end of the late Cretaceous and following collision between the Tauride and Pontide belts during the Paleocene (Arslan and Aslan, 2006; Dilek et al., 2010; Karslı et al., 2010a; Okay and Sahintürk, 1997; Topuz et al., 2005). Conversely, some authors suggest that the late Cretaceous igneous activity is related to southward subduction of Paleotethys oceanic lithosphere, based on southward migration and increasing potassium content of the magmatism over time (Bektaş et al., 1999; Eyuboglu, 2010; Eyuboglu et al., 2011b,c,d,e,f, 2014).

This study presents new and detailed geological, geochemical and chronological findings on the origin of the late Cretaceous igneous activity in the southern part of the Eastern Pontides Orogenic Belt and discusses the late Mesozoic–early Cenozoic geodynamic evolution of the eastern Mediterranean region in the light of new and old data. In addition, it provides important constraints on the accumulation rates of turbiditic sequences in fossil convergent margins.

2. Geological background

The Eastern Pontides Orogenic Belt, which is one of the essential parts of the Alpine-Himalayan belt, is located in the northeastern part of Anatolia (Fig. 1). Based on different rock assemblages, facies changes and tectonic characteristics, the belt can be divided into, from north to south, the Northern, Southern and Axial subzones extending nearly parallel to the southeastern coast of the Black Sea (Bektaş et al., 1995; Eyuboglu et al., 2006; Fig. 1). The zones are separated by E-W, NE-SW, and NW-SE trending fault zones that are also responsible for the formation of Meso-Cenozoic basins and for emplacement of magmatic rock suites and associated ores in the region (Eyuboglu et al., 2007, 2013a). In the Northern Zone, the Hercynian basement is represented by the low-grade metamorphic rocks (Boynukalın, 1991) and unmetamorphosed granitic rocks (Kaygusuz et al., 2012). The basement rocks are unconformably overlain by the volcanic and sedimentary lithologies of the early to middle Jurassic Hamurkesen Formation (Eyuboglu et al., 2014). This volcano-sedimentary unit is conformably covered by the late Jurassic–early Cretaceous limestones (Berdiga limestone). The late Cretaceous–Cenozoic time is represented mainly by

subduction-related granitic-gabbroic intrusions and volcanic-pyroclastic rocks (Eyuboglu et al., 2006, 2011b,c, 2014). The basement including high to low grade metamorphic rock bodies (mainly Pulur, Ağvanis and Tokat massifs) and the late Carboniferous unmetamorphosed granitic plutons (Köse and Gümüşhane granitoids) are well exposed in the Southern Zone (Fig. 1). The other dominant lithologies are late Triassic to early Jurassic Alaskan-type mafic-ultramafic rocks (Eyuboglu et al., 2010, 2011a), early Jurassic volcano-sedimentary units, late Jurassic to Cretaceous sedimentary rocks, late Cretaceous shoshonitic-ultrapotassic magmatics (Eyuboglu, 2010), late Paleocene to early Eocene adakitic rocks (Eyuboglu et al., 2011b,c,d,e, 2013b), and middle Eocene non-adakitic basaltic-andesitic volcanic, granitic and sedimentary rock assemblages (Eyuboglu et al., 2013a). Undated ultramafic-mafic rocks (Kop and Erzincan massifs), small metamorphic rock bodies, olistostromal ophiolitic melange of middle to late Cretaceous age, and Meso-Cenozoic sedimentary rocks are widespread in the Axial Zone (Fig. 1).

The study area is situated in the Southern Zone of the Eastern Pontides Orogenic Belt (Fig. 1). The main outcrop of Kurtoğlu metamorphics, consisting mainly of mica schists, gneisses, phyllites and metagranitic dikes, extends as a narrow ribbon along the southern border of the late Carboniferous Gümüşhane pluton. Similar lithologies, albeit on a small scale, also appear around the Melike valley and the Beyçam village at the northeast extension of the main metamorphic body. The minimum age for the metamorphic event in this unit is Carboniferous, dated as 320.3 ± 1.7 Ma (Topuz et al., 2007). This metamorphic unit is intruded by the late Carboniferous Gümüşhane and Köse granitoids that include various rock types such as granite, granodiorite, quartz diorite, rhyolite, and dacite (Dokuz, 2011; Topuz et al., 2010). The pre-Jurassic basement rocks are transgressively overlain by the early to middle Jurassic Zimonköy Formation (Figs. 1 and 2). This volcano-sedimentary unit is overlain by late Jurassic to early Cretaceous carbonates (Berdiga Formation) deposited during long-lived thermal subsidence in the entire Eastern Pontides (Fig. 2). The late Cretaceous is characterized by a thick sedimentary sequence with interlayered felsic tuffs, which are among the main objects of this study, in the Gümüşhane area (the Kermutdere Formation). On the other hand, the late Cretaceous is represented by bimodal volcanic rocks and arc-related I-type granitic intrusions about 35 km northwest of the study area (Kaygusuz et al., 2008, 2009; Kaygusuz et al., 2011). These Paleozoic and Mesozoic units are intruded by adakitic andesite and dacite porphyries (Eyuboglu et al., 2013a). The whole sequence is unconformably overlain by the early Cenozoic Alibaba Formation including basal conglomerate, Nummulite-bearing limestone, and a thick volcanic sequence consisting mainly of basalt-andesite and associated pyroclastic rocks intruded by late Eocene granitic intrusions (Arslan and Aliyazıcıoğlu, 2001; Arslan and Aslan, 2006; Eyuboglu et al., 2011b, 2013a). All of these units are cut by basic dikes representing the final stage of the Cenozoic magmatism.

3. Field characteristics and petrography

In the Gümüşhane area, late Cretaceous time is represented by the Kermutdere Formation (Fig. 2). The formation starts with yellowish colored, thin to medium-bedded sandy limestones overlying the carbonate platform (Berdiga Formation), grades upward into red pelagic limestones, and continues with sandstone, siltstone and claystone alternation, with locally interbedded felsic tuffs. However, in the southeastern part of the study area, the lower part of the Kermutdere Formation includes extensive occurrences of poorly sorted monogenic conglomerate composed of late Jurassic–early Cretaceous limestone fragments (Fig. 2).

The studied felsic tuffs are interlayered with clastic sedimentary rocks representing the upper part of the late Cretaceous Kermutdere Formation in the Gümüşhane area. However, the abundance of felsic tuff levels in the late Cretaceous sequence exhibits abrupt changes within short distances, as in most successions including pyroclastic lithologies. For example, while the late Cretaceous sequence is

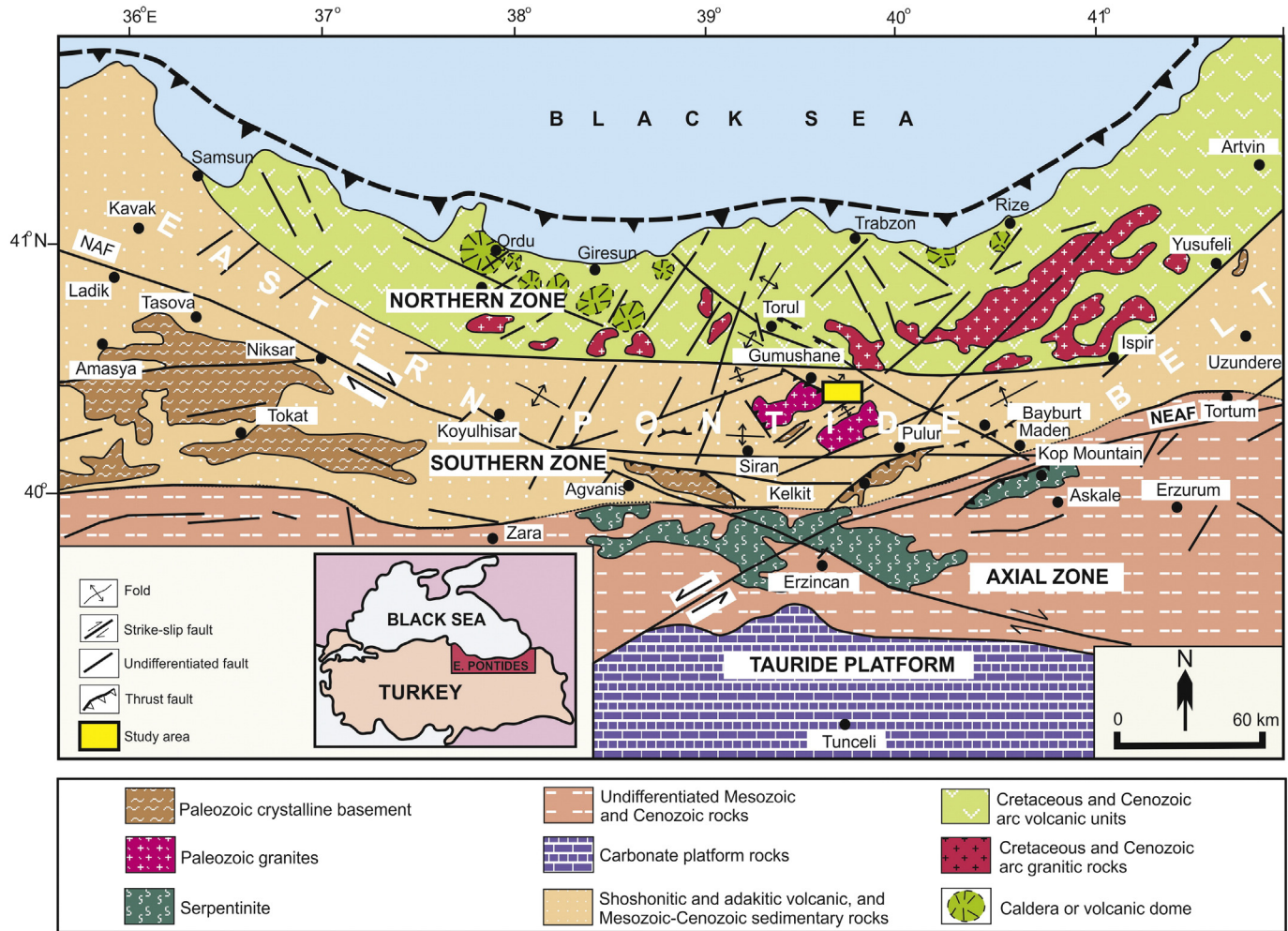


Fig. 1. Tectonic map showing the distribution of main lithological units and the zones of the Eastern Pontides Orogenic Belt.
After [Eyuboglu et al. \(2006\)](#).

dominated by felsic tuffs in the northwestern part of the study area, it includes few or no pyroclastic lithologies in the southern part of the map area (Fig. 2).

The type section of the clastic sedimentary sequence including felsic tuffs was measured on the south-facing slope of the Kazıgil Stream valley, immediately northwest of Kocapınar village (Figs. 2, 3 and 4). In this location, the clastic sequence starts with alternating sandstone, siltstone and claystone on the red limestones of the Kermutdere Formation and passes upward into a level including the first products of late Cretaceous pyroclastic activity in the study area (Fig. 4). This level, with a thickness of 8 m, is composed of cream and greenish yellow, medium- to thick-bedded felsic tuffs. Following a sandstone-dominated clastic rock alternation (28 m), the sequence grades upward into a level including ball-and-pillow structures comprising elongated, laterally stretched masses of mudstones that are surrounded by fine-grained felsic volcanic material (Fig. 4) and continues with white and cream colored, medium- to thick-bedded and felsic tuffs (15 m). After a level including mainly clastic sedimentary rocks with occasionally interbedded thin felsic tuff beds, the sequence grades upward into the thickest section of the late Cretaceous pyroclastic activity in the study area. This level, which is 39 m in thickness, starts with greenish white, thick- to massive-bedded lapilli tuffs and continues with yellowish white and white, fine grained, thick- to medium-bedded felsic tuffs. The manganese oxide dendrites and staining on some tuff beds were formed by varying groundwater oxidation state in the area. After the deposition of this thick pyroclastic level, the intensity of the felsic pyroclastic activity decreased

and the sequence passes upward into a thick clastic level consisting mainly of alternating sandstone and siltstone, which includes only two thin levels of felsic tuffs (Fig. 4). The sequence in this location is capped by conglomerate and coarse-grained sandstones of the Eocene Alibaba Formation.

Petrographic data indicate that the studied tuffs can be classified as crystal-rich and crystal-poor tuffs. The crystal-poor tuffs consist mainly of 45–65% devitrified glass shards and 10–20% broken quartz crystals, whereas the crystal-rich tuffs consist of >50% crystals of various mineralogy (mostly quartz and plagioclase).

The crystal-rich tuffs consist predominantly of large clasts of plagioclase (0.3–6 mm) and K-feldspars (0.5–2 mm). Coarse-grained plagioclase phenocrysts are partly sericitized. Most grains have embayed or sutured grain boundaries, suggesting a sudden change in P or in pressure of water in the magma just before eruption. Dark brown, almost isotropic shards (av. 1.5 mm) make up a significant part of the rock. The Fe-stained, clayey shards are interstitial to the feldspars. Their cuspatate shape distinguishes them from other Fe-stained minerals. Orthoclase phenocrysts have single twinning. They are motled and have embayed or ragged grain boundaries. Anhedral quartz clasts are broken fragments having a wide range of grain size. Anhedral carbonates occur as partial replacement after some of the minerals. The fine-grained carbonate is also interstitial to the matrix. The matrix is amorphous and consists mainly of fine-grained microcrystalline quartz, clay and amorphous Fe-hydroxide. Amphibole, biotite, apatite, zircon and titanite occur as accessory phase in the crystal-rich tuffs.

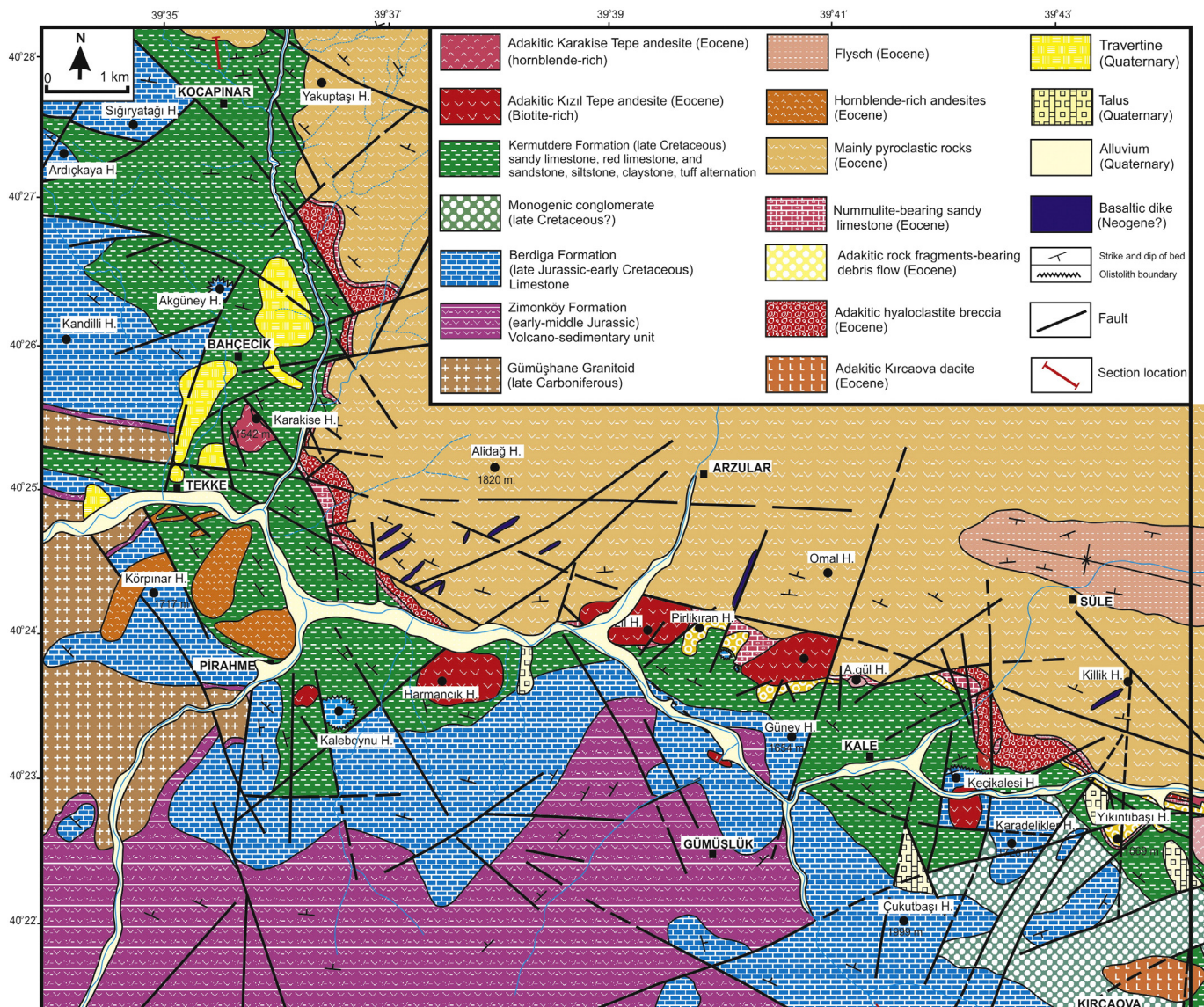


Fig. 2. The detailed geological map of the study area.
Modified from [Eyuboglu et al. \(2013a\)](#).

The crystal-poor tuffs consist mainly of devitrified shards (0.2–2.5 mm) and fine-grained quartz. Cuspate-shaped, sinuous and angular shards make up a significant part of the rock. Most shards were replaced by dark, amorphous material that contains fine-grained aggregates of rutile, minute carbonate and broken small quartz and plagioclase clasts. In addition, minute chlorite spherules are interstitial to some of the shards and also fill small vesicles. Small broken quartz clasts are interstitial to the matrix and the shards. Similarly, small broken plagioclase clasts are interstitial to the devitrified glass shards. The devitrified matrix consists predominantly of fine-grained quartz. A few grains of small, broken plagioclase phenocrysts are interstitial to the matrix, and a few small, anhedral grains of hematite also occur within the matrix. The zircon, rutile, hematite, apatite and chlorite occur as accessory phases in crystal-poor tuffs.

4. Analytical methods

In this study, in order to determine the age span of the felsic tuffs interbedded with turbidites, U-Pb isotopic analyses of zircons extracted from three felsic tuff samples, from different horizons within the late Cretaceous sequence, were performed by the SHRIMP (sensitive, high

resolution, ion-microprobe) method at the Korea Basic Science Institute (KBSI). For these analyses, the zircons were mounted in epoxy and polished to expose approximately mid-grain cross sections. Twelve individual grains were analyzed in each sample. The measured $^{206}\text{Pb}/^{238}\text{U}$ ratio was calibrated using the standard FC1 zircon (1099.0 Ma). The analytical procedures for SHRIMP dating were mostly based on [Williams \(1998\)](#). A 15–20 μm spot size was used for all analyses using a 3–4 nA negative ion oxygen beam (O_2^-). The data were collected in sets of five scans throughout the mass measurements for each element. For $^{207}\text{Pb}^*/^{206}\text{Pb}^*$ age calculations (asterisk used for the radiogenic Pb), the measured $^{204}\text{Pb}/^{206}\text{Pb}$ was used for common Pb correction. Common Pb for the $^{206}\text{Pb}^*/^{238}\text{U}$ ages was corrected on the basis of the measured $^{207}\text{Pb}/^{206}\text{Pb}$ ratio ([Williams, 1998](#)).

The whole rock major, trace and rare earth element analyses were performed on 26 samples from the felsic tuffs at ACME Analytical Laboratories, Vancouver, Canada. Of these, 11 are from the KPR measured section, and have well-constrained stratigraphic positions; the remaining 15 (KPR series) are from tuffs collected in other locations, where stratigraphic constraint is less precise. The major oxides and Sc were determined using ICP-ES, and trace and rare earth elements were analyzed by ICP-MS. The sample digestion procedures are similar

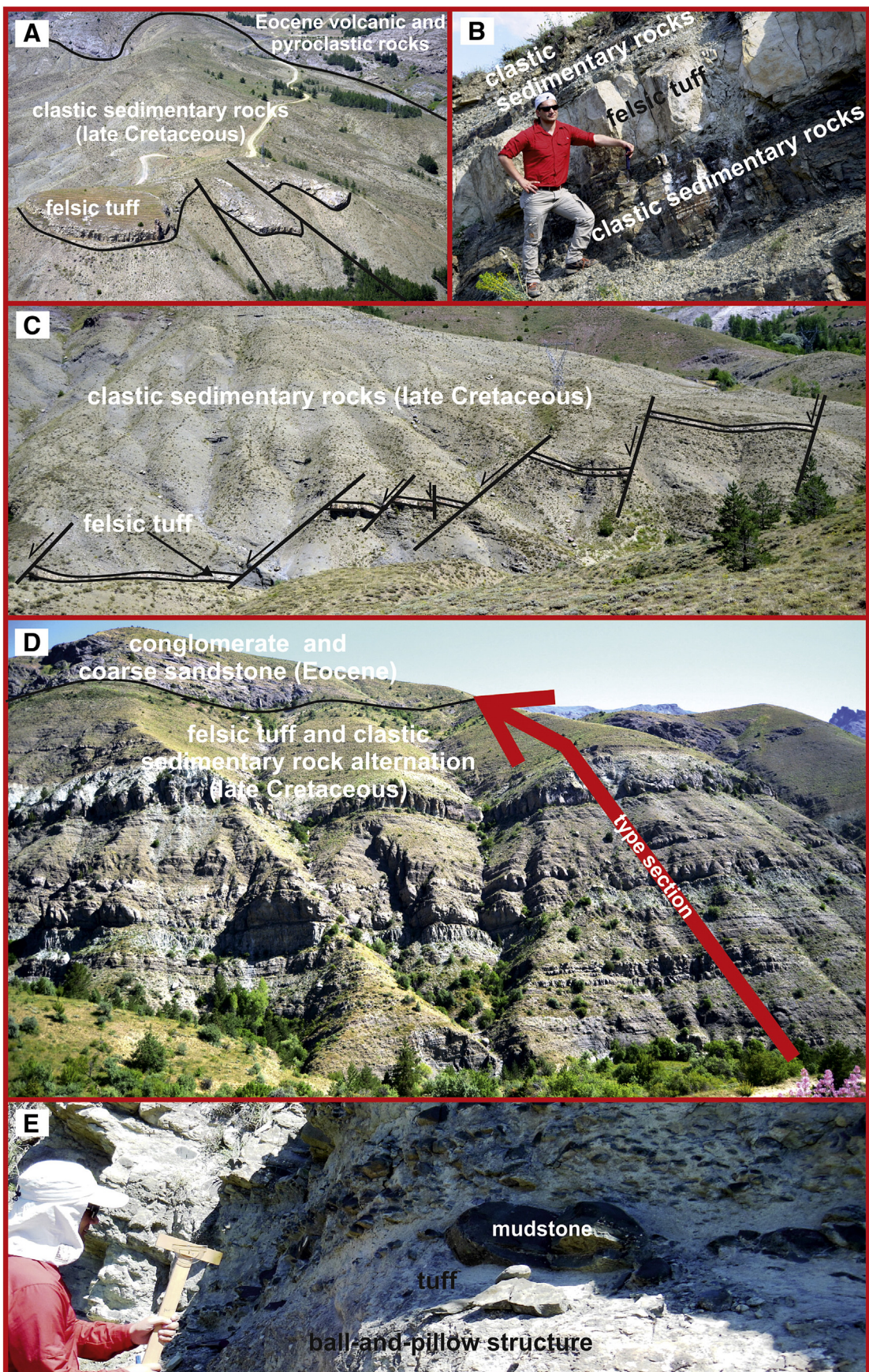


Fig. 3. The field photographs of the felsic tuffs. A) and B) Individual tuff layers within the late Cretaceous turbiditic sequence (Kale and Bahçecik areas, respectively), C) Normal faults cutting tuff and clastic rock layers (Kale area), D) Felsic tuff layers interbedded with turbidites in the type location (Kocapınar village), E) The ball-and-pillow-structures in Kermutdere tuffs (Kocapınar village).

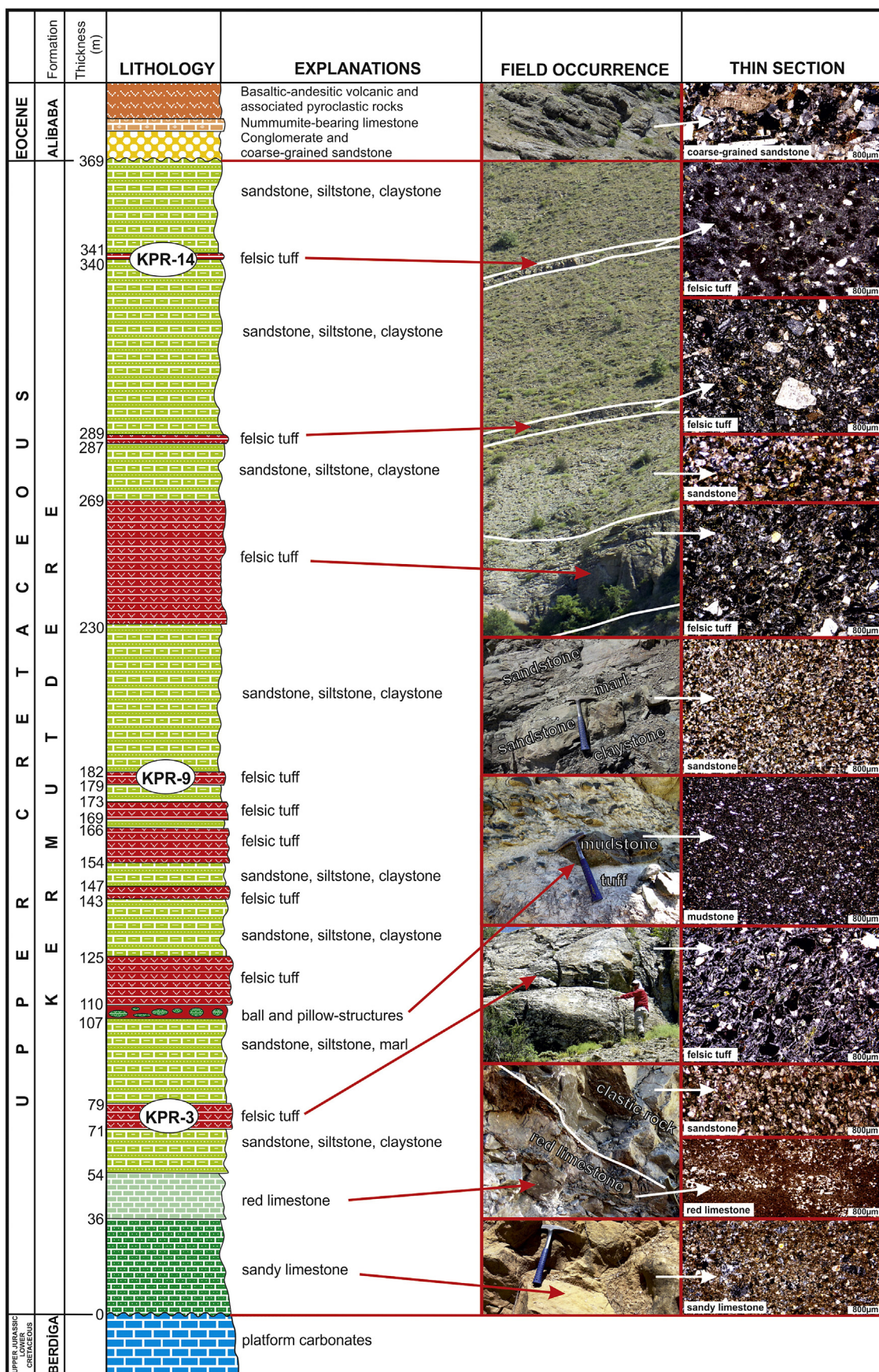


Fig. 4. Measured stratigraphic section of the Kermutdere Formation in the type location (Kocapınar village).

for both ICP-MS and ICP-ES. 0.2 g of pulverized sample is weighed into a graphite crucible and mixed with 1.5 g of LiBO₂ flux. The mixture is heated in a muffle furnace for 15 min at 1050 °C. The molten mixture is removed and quickly poured into 100 ml of 5% HNO₃. This solution is shaken for 2 h and the aliquot is transferred into a polypropylene test tube. Standards and reagent blanks are added to the sample sequence. At the second stage (sample analysis), sample solutions are aspirated into an ICP mass spectrometer (Perkin-Elmer Elan 6000) or an ICP emission spectrometer (Jarrel Ash Atomcomp Model 975) for determination of element content.

Whole-rock Sr-Nd isotope ratio analyses were performed using a VG AXIOM MC-ICP-MS after the sample powders were digested/dissolved using HClO₄ and HF in Teflon vessels at MOE Key Laboratory of Orogenic Belts and Crustal Evolution, School of Earth and Space Sciences, Peking University, Beijing, China. One unknown sample was analyzed between two standard solutions (NBS-987 for Sr, JNd_i for Nd, NBS-981 for Pb). ⁸⁷Sr/⁸⁶Sr ratios were normalized against ⁸⁸Sr/⁸⁶Sr = 0.1194 and all

⁸⁷Sr/⁸⁶Sr ratios have been adjusted to NBS-987 Sr standard = 0.710250. ¹⁴³Nd/¹⁴⁴Nd ratios were normalized against ¹⁴⁶Nd/¹⁴⁴Nd = 0.7219, and have been adjusted to JNd_i standard = 0.512115.

5. Results

5.1. Zircon chronology

Abundant zircons were recovered from all three samples processed for U-Pb dating (Fig. 5). The zircons are euhedral and equant, or stubby prisms with aspect ratio less than 3. Many show strong zoning in cathodoluminescence (CL) images, which is usually interpreted as primary igneous zoning (Fig. 5). Most zircons are brightly luminescent, and many have dark cores; it is not clear whether these dark cores are remnants of inherited zircon or simply the earliest magmatic zircon formed in these tuffs. Some show sector zoning. The zircons are mostly small, with only few exceeding 100 µm, but the equant morphology

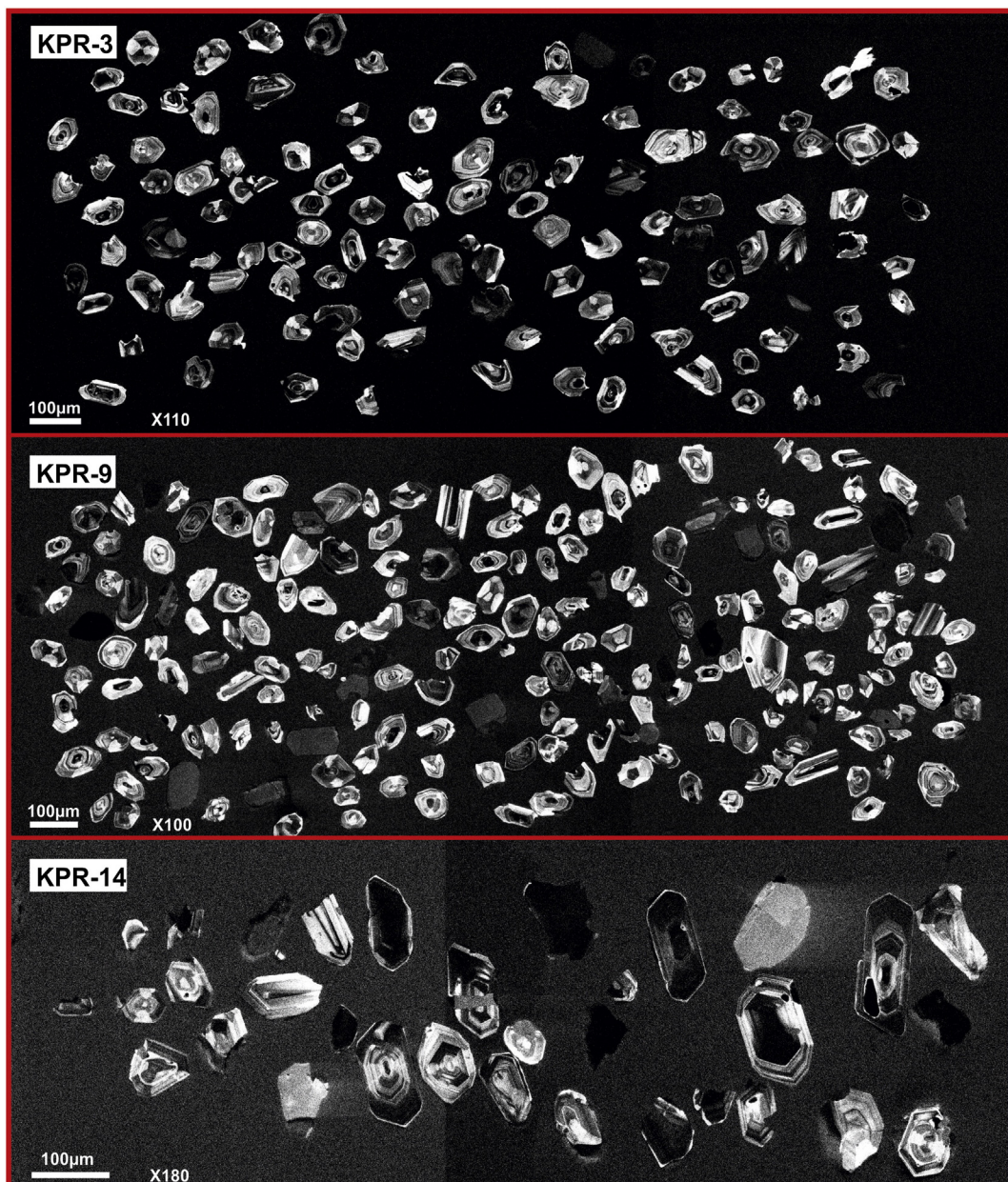


Fig. 5. CL images of zircons extracted from samples KPR-3, KPR-9 and KPR-14.

assures that spot sizes of $\sim 20 \mu\text{m}$ are appropriate. Fewer zircons were recovered from KPR-14; these are somewhat larger than those in samples KPR-3 and KPR-9, and are mostly prismatic.

The Th/U ratios of analyzed zircons range from 0.36 to 1.56 (Supplementary table), and these high values are consistent with a magmatic origin (Rubatto, 2002). The U-Pb data show three statistically distinct ages

at 84, 81 and 77 Ma (Supplementary table; Fig. 6), with uncertainties of about 1 Ma. The ages are consistent with stratigraphic relations, and indicate that tuff-forming magmatism was episodically active over a minimum of 7 Ma. Data for two grains in KPR-14, with large uncertainties, lie slightly above the cluster of other data, and may possibly reflect inheritance of older zircons.

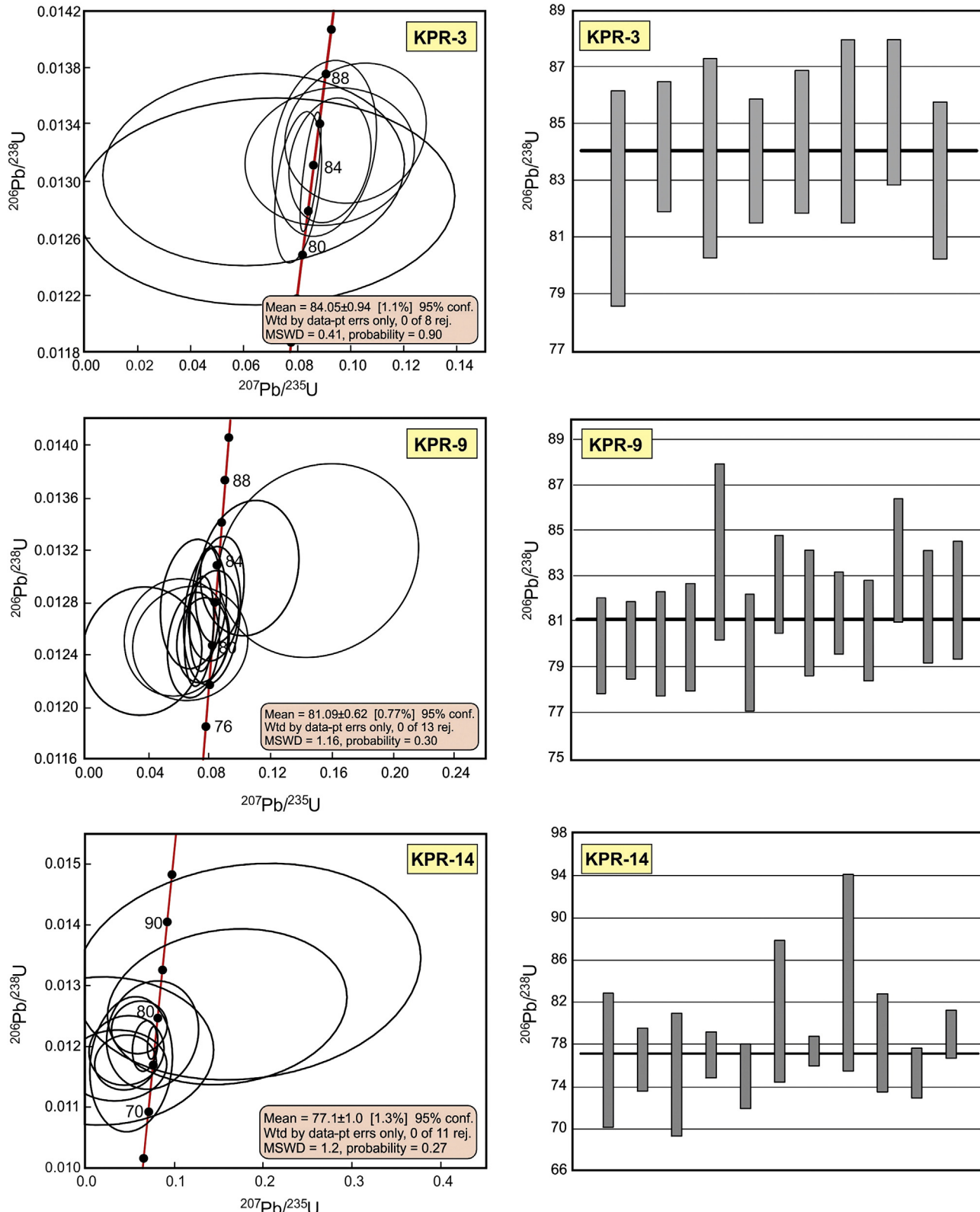


Fig. 6. Concordia diagrams showing U-Pb analyses of zircons from three tuff layers within the turbiditic sequence in Kocapinar village (Tekke, Gumushane).

5.2. Geochemistry

5.2.1. Whole rock geochemistry

The tuffs are characterized by high Na₂O (2.23–6.12 wt.%), SiO₂ (64.5–78.38 wt.%), Zr (68.8–183.3 ppm), Th (10.3–22.1 ppm), and U (2.8–6.1 ppm), low TiO₂ (0.13–0.44 wt.%), Fe₂O₃ (0.9–3.05 wt.%), CaO (0.31–3.19 wt.%), MgO (0.34–2.28 wt.%), Co (0.3–6.2 ppm), Ni (1–36.8 ppm), and Sr (18–144.4 ppm), and moderate Al₂O₃ (9.69–13.44 wt.%) contents (Table 1). They display a wide range of K₂O (0.41–4.62 wt.%). On a total alkali–silica chemical classification diagram (TAS), the studied tuffs fall into rhyolite and dacite fields with their high SiO₂ contents (Fig. 7A). Similarly, on a Zr/TiO₂ versus Nb/Y nomenclature diagram (Winchester and Floyd, 1977), which uses relatively immobile elements, they plot in the field of dacite/rhyodacite supporting their felsic nature (Fig. 7B). The studied felsic tuffs exhibit a wide distribution pattern covering tholeiitic, calc-alkaline, high-K calc-alkaline and shoshonitic fields on a K₂O versus SiO₂ diagram (Fig. 7C), suggesting the effects of hydrothermal alteration on them. On a Th–Co diagram (Fig. 7D), which is valuable for altered and intensely weathered volcanic and pyroclastic rocks, all of the analyzed samples fall into high-K and shoshonitic rock field in affinity with their high Th contents (10.3–22.1 ppm) and dacite/rhyodacite field in composition with their low Co contents (0.3–6.2 ppm). The studied felsic tuffs are peraluminous, except for four samples that are weakly metaluminous. They also exhibit the chemical characteristics of arc-related non-adakitic igneous rocks with their low Sr and moderate to high Y contents. The studied felsic tuffs fall in the high-K calc-alkaline and shoshonitic fields on the Th/Yb versus Ta/Yb discrimination diagram (Fig. 8A). They also plot in the volcanic arc granite (VAG) field on the Ta versus Yb diagram (Fig. 8B).

The LOI of the analyzed samples ranges from 3.2 to 7 wt.% (Table 1). At this level of alteration, it is difficult to find reliable criteria for classification of rock types and even of rock series. Thus, for example, SiO₂ and K₂O decrease with increasing LOI, whereas Al₂O₃ and Na₂O increase with LOI; CaO shows no consistent pattern of change with LOI. In the absence of unaltered equivalents, it is difficult to determine what the initial Na₂O and K₂O of these rocks might have been. The elevated SiO₂ content of these tuffs (>65 wt.%) and the abundance of plagioclase compared with K-feldspar suggest that these are dominantly dacitic or rhyodacitic tuffs. The thin tuff beds also indicate that these are dominantly air-fall, rather than ash-flow tuffs.

The mantle-normalized trace element patterns (Fig. 9A) show relative depletions of the high field strength elements (HFSE; Nb, Ta, Zr, Hf, Ti); these are consistent with the arc volcanic setting of these rocks, if we assume that these elements have been mostly immobile. The extreme enrichment of Pb is typical of continental arc volcanics, but could also reflect Pb mobility during alteration. In contrast to the relatively large scatter in the concentrations of most trace elements, the Sr content of these rocks is uniformly low. This may be due to Sr removal by early crystallization of plagioclase, or to Sr loss during alteration of plagioclase. Correlation of Sr with LOI is not statistically significant. There is thus ambiguity in interpreting trace element patterns. The distribution of Ni is unusual, in that Ni concentrations above 10 ppm are atypical of felsic (i.e., dacitic to rhyolitic) rocks, and 12 of 26 samples have Ni above 10 ppm, with a maximum of 36.8 ppm. Other trace elements that are usually enriched in mafic rocks (Cr, Co) show enrichments similar to Ni. These enrichments characterize most KTF samples, but not the KPR samples.

Because rare earth elements (REE) are less mobile during alteration than many other trace elements, the concentrations of REE (Fig. 9B) show less scatter than those of other trace elements. Thus, for example, the coefficient of variations (cv; ratio of the standard deviation to the mean value) for Ba and Rb are 0.75 and 0.66 (0.57 for K₂O), respectively, compared with cv of <0.15 for all of the light REE. However, the positive correlations of La, Ce, and Pr with LOI are statistically significant, indicating that even the light REE have been affected by alteration. Chondrite-normalized REE patterns are typical of felsic, arc volcanic rocks, showing

light REE enrichment, negative Eu anomalies, and flat heavy REE profiles with chondrite-normalized abundances averaging near 10 (Fig. 9B). Overall REE concentrations vary by a factor of two to three, with a larger relative range in the heavy REE. Some samples show a slightly concave profile among the heavy REE.

5.2.2. Sr–Nd–Pb Isotope chemistry

Six samples were analyzed for their whole rock Nd, Sr, and Pb isotopic compositions at Peking University (Beijing, China) and initial ratios were calculated using an age of 80 Ma (Campanian). Because parent/daughter for the isotopic systems was calculated from bulk rock elemental concentrations, and not from parent/daughter measured by isotope dilution on the same powders that were processed for isotopic ratios, the radiogenic ingrowth corrections are relatively imprecise. Thus, for example, U abundances were determined only to two significant figures, and the other elemental abundances only to three significant figures. The results indicate that the studied felsic tuffs are characterized by relatively low initial ratios of ¹⁴³Nd/¹⁴⁴Nd (0.512296–0.512484; ε_{Nd} : −2.1 and −7.2) and ⁸⁷Sr/⁸⁶Sr (0.704896–0.706159; Fig. 10). Their initial Pb isotopic compositions range from 18.604 to 18.646 for ²⁰⁶Pb/²⁰⁴Pb, from 15.644 to 15.654 for ²⁰⁷Pb/²⁰⁶Pb and from 38.712 to 38.763 for ²⁰⁸Pb/²⁰⁴Pb (Table 2; Fig. 10). They have depleted mantle Nd model ages (T_{DM}) ranging between 0.89 and 1.29 Ga (Table 2).

There are no systematics in the isotopic data. Isotopic compositions do not correlate with parent/daughter, or with inverse elemental concentrations, which, in closed isotopic systems, would allow calculations of isochrons or mixing models, respectively. The isotopic data do not correlate with SiO₂ content or immobile trace element content (e.g., Zr). Among the isotopic data, it is possible that only the Sm–Nd data approximate those of the original igneous rocks, and that the other data map the characteristics of the alteration environment.

6. Discussion

6.1. Petrogenesis

Extensive alteration of the tuffs makes interpretation of their petrogenesis difficult and ambiguous. Individual tuff layers are thin, mostly <2 m in thickness, implying that these are either distal portions of larger tuff units, or that they are products of relatively small, locally-sourced eruptions. The absence of thick and widespread, tuff-dominated, volcanic formations in the Gümüşhane area, such as would be associated with major caldera-forming eruptions, thus suggests that the tuffs of the Kermutdere Formation are due to small-scale eruptions from local sources. The thickest tuff in the measured section is 39 m; assuming that this represents the original thickness, and assuming that the areal extent of this tuff is ~100 km², the total erupted volume for this unit is only 3.9 km³ – small compared with most pyroclastic eruptions.

The tuffs formed over at least 7 Ma, between 84 and 77 Ma. It is possible that undated tuff horizons may be somewhat older or somewhat younger than this range. Small magma chambers are unlikely to persist over periods of several Ma, so that these tuffs are interpreted to be the products of discrete eruptions from several different magma bodies. There is therefore no expectation that the geochemical characteristics of these tuffs should be uniform or systematically related. The general tectonic setting, that of a convergent margin with associated arc-type magmatism, provides the framework within which the geochemistry of these tuffs can be interpreted.

Discrimination of the magma series to which these tuffs might belong, based on major elements, is difficult. The major magma series – tholeiitic, calc-alkaline, high-K calc-alkaline, and shoshonitic – are usually discriminated primarily on K₂O vs. SiO₂, or total alkali vs. SiO₂ diagrams. In this case, the alkali elements and SiO₂ are clearly modified by alteration, so that these diagrams are not reliable. The classification of magma series by trace elements is equally unsatisfactory because it is difficult to demonstrate that trace elements have been immobile

Table 1

Major, trace and rare earth element concentrations of the felsic tuffs.

Sample	KTF-2	KTF-3	KTF-5	KTF-7	KTF-9	KTF-10	KTF-11	KTF-13	KTF-14	KTF-15	KTF-16	KTF-17	KTF-18	KTF-24
SiO ₂	75.72	73.8	78.38	71.45	66.53	70.12	64.5	69.74	71.28	69.5	69.08	70.71	69.9	68.63
TiO ₂	0.2	0.2	0.17	0.2	0.39	0.27	0.44	0.33	0.32	0.3	0.29	0.31	0.29	0.23
Al ₂ O ₃	10.94	11.4	9.69	11.94	12.41	11.63	13.24	12.97	11.64	12.58	12.91	11.47	12.17	13.18
Fe ₂ O ₃	1.18	1.54	0.94	1.31	2.98	2.2	3.05	2.27	2.34	2.23	2.18	2.31	2.3	1.56
MnO	0.01	0.02	0.01	0.02	0.05	0.04	0.06	0.05	0.05	0.05	0.05	0.05	0.05	0.02
MgO	0.93	1.46	0.82	1.25	2.28	1.41	2.27	1.07	1.09	1.1	1.07	1.12	1.19	1.36
CaO	0.41	0.54	0.31	1.52	3.4	2.67	3.74	1.87	2.15	1.87	1.88	2.36	2.24	1.79
Na ₂ O	3.2	3.04	3.64	4.42	2.23	3.99	4.74	4.72	4.04	4.89	4.87	4.45	4.25	5.36
K ₂ O	4.03	4.51	2.32	3.83	4.62	1.76	3.19	1.62	1.98	1.5	1.9	1.34	2.16	1.27
P ₂ O ₅	0.05	0.04	0.03	0.05	0.06	0.04	0.07	0.06	0.06	0.06	0.05	0.06	0.05	0.04
Cr ₂ O ₃	0.005	0.01	0.004	<0.002	0.027	0.014	0.021	0.015	0.016	0.012	0.013	0.014	0.016	0.003
LOI	3.2	3.3	3.6	3.8	4.8	5.7	4.4	5.2	4.9	5.8	5.6	5.7	5.2	6.5
Total	99.88	99.87	99.91	99.79	99.78	99.84	99.72	99.92	99.87	99.89	99.89	99.89	99.83	99.94
Mg #	61.0	65.3	63.3	65.4	60.2	55.9	59.6	48.3	48.0	49.4	49.3	49.0	50.6	63.3
Sc	4	4	3	4	8	7	9	7	8	7	7	7	7	4
V	11	11	<8	15	42	30	45	33	35	28	29	35	30	8
Co	1.8	3.8	0.6	0.5	5.9	4.1	6.2	3.8	4.2	3.3	3.6	4.4	3.5	1.1
Ni	11.2	33	3.1	3	36.8	25	35.1	23.7	25.8	18.1	22.6	26.3	19.5	3.6
Cr	34.3	41.1	27.4		185.1	96.0	144.0	102.8	109.7	82.3	89.1	96.0	109.7	20.6
Cu	8.6	29.6	2.6	1.8	20.8	7.8	7.2	5.3	5.2	5.4	5.1	5.5	4.4	2.8
Zn	33	34	24	29	46	39	49	42	41	39	43	39	43	34
Ga	8.4	9	6.8	9.1	12.1	11	12.5	11.3	12.1	12.1	11.4	11.6	11.6	9.3
Cs	22.6	22.2	27.3	1	8.4	26.5	1.9	20.8	16.3	20	19.1	18.1	17.5	13.8
Rb	78.1	84.2	72.4	264.2	156.2	60.9	206.3	60.3	75.7	52.8	66.9	49.2	81.7	37.9
Ba	953	783	421	1465	1040	433	1324	473	528	363	460	340	668	294
Sr	83.2	94.6	18	35.2	121.7	79.2	140.7	90.1	77.8	74.2	74	74.5	79.9	65.5
Y	25.3	23.9	21.3	25.8	18.3	18.6	20.5	20.2	19.1	19.3	19.5	17.9	20.1	27.4
Zr	135.6	136	115.5	138.8	166.4	131	183.3	171.9	146.1	154.8	143.9	133.1	152.9	174.8
Nb	10.6	10.3	8.5	9.1	11	10.7	12.3	11.8	10.9	11.5	11.8	10.4	10.8	11.8
Hf	3.5	3.8	3	3.6	4.9	3.8	5.3	4.7	4	4.2	4	4.1	4.9	5.3
Ta	0.7	0.6	0.7	0.7	0.9	1	0.9	1.1	1	1	1	0.9	1	0.8
Pb	27.3	27.7	26.3	27.4	25.7	29	26.9	31.9	29.2	31.8	30.8	27.6	30.8	29.6
Th	13.2	13.9	11.5	13	15.3	18.4	16.3	18.5	18.2	18.2	20.2	17.9	20	16.8
U	3.9	3.7	2.9	4	4.8	4.8	5.4	5.4	5.3	5.5	5	5.3	5.4	4.8
La	32.6	31.8	23.4	25.1	36.9	35.3	39.4	37.6	37.4	39.9	39	35.1	39.7	39.6
Ce	61	56.7	45.2	49.3	66.3	64.2	67.9	66.9	66.1	68.1	70.1	65.5	71.4	72
Pr	6.12	6.07	4.79	5.61	6.99	6.42	7.13	7	6.83	7.15	7.16	6.58	7.28	7.63
Nd	21.2	19.4	18.8	19.6	22.6	21.3	24.9	23.6	23.8	24.5	23.6	20.3	25.1	26.2
Sm	4.1	3.99	3.49	4	4.09	3.54	4.55	4.16	4.11	4.3	4.2	3.81	4.55	5.12
Eu	0.69	0.67	0.57	0.75	0.85	0.65	0.97	0.79	0.73	0.76	0.69	0.71	0.77	0.93
Gd	3.69	4.02	3.13	4.02	3.55	3.35	3.78	3.57	3.36	3.83	3.82	3.58	3.8	4.84
Tb	0.69	0.69	0.57	0.73	0.59	0.56	0.66	0.62	0.6	0.61	0.6	0.6	0.62	0.81
Dy	3.72	3.88	3.51	4.4	3.23	3	3.28	3.55	3.28	3.39	3.75	3.52	3.62	4.54
Ho	0.93	0.91	0.8	0.92	0.69	0.68	0.73	0.74	0.68	0.76	0.68	0.76	0.75	1.04
Er	2.85	2.79	2.57	2.96	2.01	2.18	2.25	2.14	2.08	2.16	2.14	1.88	2.34	3.1
Tm	0.47	0.45	0.41	0.5	0.33	0.3	0.35	0.34	0.34	0.34	0.33	0.32	0.35	0.49
Yb	3.07	3.03	2.71	3.22	2.12	2.14	2.33	2.39	1.96	2.22	2.27	2.03	2.3	3.16
Lu	0.49	0.45	0.4	0.5	0.36	0.31	0.35	0.35	0.32	0.34	0.38	0.35	0.34	0.52
Sr/Y	1.1	1.1	0.8	1.4	6.7	4.3	6.9	4.5	4.1	3.8	3.8	4.2	4.0	2.4
(La/Yb) _N	7.2	7.1	5.8	5.3	11.7	11.1	11.4	10.6	12.9	12.1	11.6	11.7	11.6	8.4

under the conditions of major element alteration. The evident difficulties with both Th and Co data, noted above, make discrimination on the Th vs. Co diagram (Fig. 7D) and the Th/Yb vs. Ta/Yb diagram (Fig. 8A) suspect. The displacement of the Kermutdere samples from the calc-alkaline field on Fig. 8A can be interpreted as being due to Th enrichment during alteration. The flat heavy REE patterns of the tuffs contrast with the sloping heavy REE profiles of some shoshonites in the Eastern Pontides (Eyuboglu et al., 2010), and suggest that a shoshonitic affinity is unlikely. Similarly, the heavy REE contents are low compared with most evolved or fractionated tholeiitic rocks (Fig. 9B). The tuffs may belong to either the calc-alkaline or high-K calc-alkaline series.

The least altered samples (LOI ~ 3 wt.%) have SiO₂ near 75 wt.% and K₂O near 4 wt.%, with K₂O exceeding Na₂O. These data do not accord with the petrographic observation that plagioclase in these rocks is more abundant than K-feldspar; SiO₂-rich, rhyolitic rocks typically have K-feldspar as the dominant feldspar. Because the plagioclase-to-K-feldspar ratio can be petrographically quantified, even in most altered rocks, it may be a better measure of rock type, and this criterion would indicate that these rocks are dacitic or rhyodacitic.

It is well known that the subduction-related continental arc magmas are characterized by high contents of LIL and LRE elements relative to HFS and HRE elements, respectively, negative anomalies of Nb, Ta, Zr, and Ti, and also an abundance of hydrous minerals such as biotite and amphibole (e.g., Eyuboglu et al., 2010; Gill, 1981; Hawkesworth et al., 1991; Murphy, 2007; Ringwood, 1990). On the primitive mantle and chondrite-normalized distribution diagrams (Fig. 9A and B), enrichment in LIL and LRE elements relative to HFS and HRE elements, strong negative Nb, Ta and Ti anomalies, and also the existence of primary biotite crystals suggest a subduction-related setting for the origin of the studied felsic tuffs.

The roles of important petrogenetic processes, like partial melting and fractional crystallization, cannot easily be assessed. It is likely that there is variation in major element compositions in these tuffs that is due to petrogenetic processes other than alteration, but it is difficult to demonstrate this. Because there are no low-SiO₂ rocks in this suite, it is not possible to describe a fractional crystallization trend based on the major elements.

The relatively immobile trace elements – the HFSE and REE – have a range of abundances that varies by a factor of two to three. A single

KTF-25	KPR-1	KPR-2A	KPR-3	KPR-4	KPR-5	KPR-6	KPR-9	KPR-10	KPR-12B	KPR-13B	KPR-14
69.45	73.29	72.93	74.62	76.69	73.92	72.18	76.6	70.07	72.2	69.32	67.45
0.21	0.27	0.2	0.22	0.25	0.25	0.22	0.29	0.2	0.15	0.14	0.13
12.52	11.39	12.09	11.97	11.12	12.35	11.77	10.1	11.56	12.72	14.27	13.44
1.52	2.32	1.73	0.99	0.99	1.15	1.11	1.17	1.72	1.14	1.36	0.9
0.01	0.03	0.04	0.01	0.01	0.02	<0.01	0.02	0.07	0.02	0.04	0.02
1.33	1.21	0.83	0.5	0.34	0.52	0.43	0.48	0.82	0.49	0.72	0.58
1.92	0.74	0.79	0.46	0.47	0.47	1.81	1.39	3.19	0.38	0.43	2.89
5.39	4.66	5.52	5.65	4.25	4.17	2.99	3.49	3.66	5.15	6.12	6.55
0.87	0.67	0.61	0.41	1.7	2.12	2.37	2.11	2.7	1.84	1.04	0.93
0.03	0.05	0.04	0.05	0.05	0.04	0.05	0.05	0.05	0.03	0.03	0.02
<0.002	0.015	0.007	0.007	<0.002	0.003	<0.002	0.006	0.004	0.004	<0.002	0.005
6.6	5.1	5.1	5.1	4	4.9	6.7	4.2	5.9	5.8	6.5	7
99.85	99.75	99.89	99.99	99.87	99.91	99.63	99.91	99.94	99.92	99.97	99.92
63.4	50.8	48.7	50.0	40.5	47.3	43.4	44.8	48.6	46.0	51.2	56.1
4	6	5	4	4	4	4	6	3	3	3	2
<8	27	14	<8	<8	<8	<8	24	14	<8	<8	<8
0.8	3.3	2.1	0.7	0.4	0.5	0.3	1.5	1.7	0.7	0.5	1.5
2.7	16.5	8.7	1.8	1.9	1.4	1	4.3	5.8	2.6	2.4	6.1
	102.8	48.0	48.0		20.6		41.1	27.4	27.4		34.3
2.4	2.7	10.3	4.3	2.7	2.2	2.1	5.9	6.9	3.4	3.3	3.7
34	42	38	24	24	21	15	29	31	16	35	19
12.6	9.8	10.4	8.7	8.5	10.4	10.9	6.1	9.6	10.1	11	5
13.6	6.5	6.8	6.1	5.3	5.7	1	5.4	7.1	10.5	13.6	20.1
30.7	31.6	35.4	24.2	70.6	84.5	113.7	67.8	87.5	74.7	43.5	26.6
225	1425	242	89	379	410	1790	435	448	329	175	170
50.8	90.1	67	38.6	59.8	62.9	144.4	67.2	92.9	93.7	47.4	52
26.1	17.9	18.1	23	24.6	26.3	25.4	21	14.7	14.7	16.4	9.2
164.7	131.1	136.9	142.6	152.1	154.7	143	117.3	122.7	112.7	111.4	68.8
12	10.7	10.6	9.2	9.1	9.9	9.4	6.8	6.3	7.7	7.7	7
5.2	3.4	3.8	4	4.3	4.5	4.9	3.1	3.1	3.3	3.2	2.3
0.9	0.9	0.9	0.7	0.6	0.9	0.7	0.6	0.5	0.6	0.7	0.6
28.8	30.5	31.9	22.5	19.7	20.7	18.9	16.4	28.8	22.4	27.5	35.8
17.8	18.2	19.3	12.9	12.9	14.1	14.2	10.3	15.2	19.7	22.1	21.7
4.7	5.2	5.5	3.8	5.1	3.9	2.8	2.7	4.8	6	5.1	6.1
41.5	35.5	36.9	32.1	31.3	33.7	35.3	23.9	32.2	37.2	39.3	27.8
72.8	65.2	63.4	58.9	57.2	61.8	63.8	43.7	54	59.3	64.8	44.8
7.93	6.54	6.83	6.23	6	6.57	6.91	4.68	5.06	5.81	6.1	4.58
27.3	22.7	22.4	21.1	21.4	25.2	23.6	15.4	16.9	18.9	20.1	14.2
5.03	3.89	3.83	4.14	3.91	4.5	4.56	3.26	2.88	3.14	3.18	2.3
0.93	0.62	0.6	0.71	0.75	0.79	0.74	0.66	0.56	0.5	0.54	0.41
4.56	3.27	3.29	3.78	3.8	4.07	4.14	3.21	2.52	2.33	2.59	1.89
0.78	0.55	0.56	0.66	0.67	0.73	0.72	0.57	0.41	0.4	0.42	0.3
4.59	3.22	3.38	4.03	3.99	4.49	4.18	3.3	2.22	2.21	2.46	1.84
0.94	0.7	0.7	0.84	0.84	0.97	1	0.78	0.48	0.55	0.55	0.41
3.03	2.05	1.95	2.58	2.92	2.97	3.07	2.31	1.63	1.71	1.86	1.28
0.48	0.31	0.32	0.41	0.45	0.45	0.49	0.35	0.26	0.27	0.3	0.2
3.27	1.92	2.12	2.71	2.82	3.27	3.08	2.3	1.81	1.91	2.12	1.42
0.5	0.32	0.34	0.45	0.47	0.49	0.54	0.36	0.33	0.33	0.35	0.22
1.9	5.0	3.7	1.7	2.4	2.4	5.7	3.2	6.3	6.4	2.9	5.7
8.6	12.5	11.7	8.0	7.5	6.9	7.7	7.0	12.0	13.1	12.5	13.2

ample, KPR-14, because of its low HFSE and REE content, accounts for much of this variation, and KPR-14 may need to be treated separately. The range of variation of the least mobile trace elements places broad limits on fractional crystallization and partial melting. Fractional crystallization alone is unlikely to produce changes in incompatible element concentrations that exceed a factor of 2. In the limiting, ideal case of Rayleigh fractionation, with bulk distribution coefficients typical of incompatible elements ($D < 0.1$), 50% crystallization would be required to produce a two-fold concentration increase, and 70% crystallization would be required to produce a three-fold change in concentration. There is no evidence to support such degrees of fractionation between samples of these tuffs, yet the HREE, for example, range in concentration by a factor of two (excluding data for KPR-14). It is thus likely that variable degrees of partial melting, combined with some degree of fractional crystallization – likely less than 50% – can explain the variation of immobile trace element concentrations.

The remarkable similarity of the REE profiles, at different concentrations, indicates that the original source material for all of the tuffs was similar. Large negative Eu anomalies show that plagioclase played a major role in the evolution of the magmas, either as a crystallizing

phase, or as a residual phase in their source. Three samples have slightly concave profiles in the heavy REE range (Fig. 9B). This indicates that some fractionation of amphibole occurred during evolution of these magmas, or that amphibole could have been a residual phase during partial melting. The subtle differences in the heavy REE profiles – some flat, some concave – show that the tuff samples have somewhat different petrogenetic histories.

Because of the apparent mobility of Rb, Sr, Th, and Pb, the isotopic compositions of the Sr and Pb systems carry little petrogenetic information. Age-corrected Sr isotopic compositions appear to be offset to lower $^{87}\text{Sr}/^{86}\text{Sr}$ than most other Eastern Pontide rocks of similar age. This implies perturbation of Rb/Sr early in the history of these rocks. The low Sr isotopic compositions are inconsistent with the low $^{143}\text{Nd}/^{144}\text{Nd}$ of these samples. Assuming a simple model of mixing between a depleted component and a radiogenic crustal component, low Nd isotopic compositions should be accompanied by increasingly radiogenic Sr isotopic compositions. Late Cretaceous subvolcanic rocks in the Maçka area (Aydin, 2014), approximately 50 km to the north of the study area, have Nd isotopic compositions similar to those of the Kermutdere

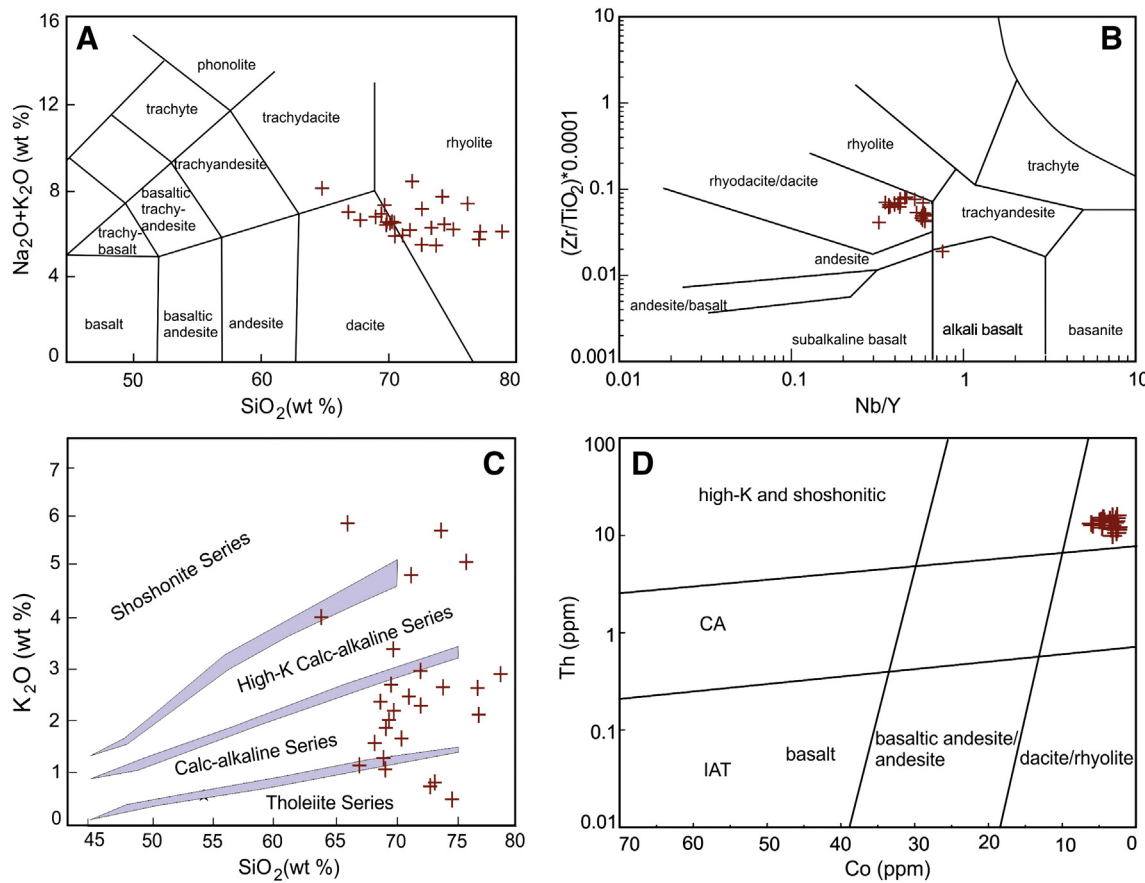


Fig. 7. Chemical nomenclature and classification diagrams for the felsic tuffs (A: after LeBas et al., 1986; B: after Winchester and Floyd, 1977; C: after Rickwood, 1989; D: after Hastie et al., 2007).

tuffs, and $^{87}\text{Sr}/^{86}\text{Sr}$ near 0.7085; these compositions are consistent with other data from the Eastern Pontides (Fig. 10). These tuffs and the Maçka subvolcanic rocks document, for the first time in the Eastern Pontides for the late Cretaceous time, the occurrence of an isotopic component with very low Nd isotopic compositions. It is not clear whether this isotopic composition is related to old, enriched mantle, or to sources in the lower crust, although Aydin (2014) interprets the Nd data as evidence of mixing between lower crustal and mantle magmas. The Kermutdere data do not provide additional constraints on this interpretation.

The distribution of Sr-Nd isotopic compositions in late Cretaceous igneous rocks of the Eastern Pontides (Fig. 10A) is consistent with two-component mixing between depleted mantle and crust. By contrast, the Pb isotopic data for this same suite of rocks are not compatible with two-component mixing (Fig. 10B and C), and require at least a third component. The reservoir from which this third component derives, and its composition, are poorly constrained.

The scatter of Sr isotopic compositions contrasts with the tight clustering of the Pb isotopic data. This clustering can be interpreted either as reflecting a remarkable uniformity in U/Pb and Th/Pb over the ~80 Ma history of these rocks, or as indicating relatively recent exchange of Pb between the rocks and their surroundings. The latter interpretation is more likely, particularly because the Nd isotopic data show a wide range. The contrasting patterns of the Sr and Pb isotopes are consistent with a history of early alteration of Rb/Sr, U/Pb, and Th/Pb, and a recent history of Pb exchange.

It is tempting to posit a genetic relation between the Maçka subvolcanic rocks and the studied tuffs, primarily because they share the same unusual range of Nd isotopic compositions. The hypothesis that the subvolcanic rocks are a less fractionated representative of the same magmatic event that produced the tuffs is also consistent with

their similarities in age. The subvolcanic rocks are metaluminous, whereas the tuffs are peraluminous; this potentially reflects the depletion of alkali and alkaline earth metals during alteration of the tuffs. The average abundances of the HFSE and REE in the tuffs are 1.5–2 times those of the average of the subvolcanic rocks, implying that, if fractional crystallization is solely responsible for the chemical differences between these rocks, the tuffs would be products of 50–70% crystallization of a tonalitic precursor. A major difficulty is that the Maçka subvolcanic rocks, as presently exposed, are also very small volume intrusions, and no large magma body of similar chemistry and age is known in this area of the Eastern Pontides.

6.2. Basin evolution and accumulation rate

Detailed geological and geophysical studies indicate that two periods of basin development can be distinguished in the Eastern Pontides Orogenic Belt during the Mesozoic (Bektaş et al., 1995, 1999; Eyuboglu et al., 2006; Yilmaz, 2002). The first period is represented by rift-related basins that formed as a result of a polyphase extensional tectonic regime during the early to middle Jurassic (Eyuboglu et al., 2006). The field studies in the southern part of the Eastern Pontides Orogenic Belt indicate that the subsidence of Jurassic rift basins occurred in three stages. The initial phase of tectonic subsidence is characterized by the formation of asymmetric half grabens and accumulation of coarse clastics and bimodal extrusive rocks (Fig. 11). In the subsequent phase, these rift-related basins experienced short-term thermal subsidence resulting in the deposition of the condensed, pelagic, red Ammonitico-Rosso limestone that is widespread in the Jurassic rift-related basins in the Alpine-Himalayan belt. Recurrent tectonic subsidence as a result of the second rifting process in Jurassic time deepened the rift-related basins in which epiclastic sediments and extrusive rocks accumulated

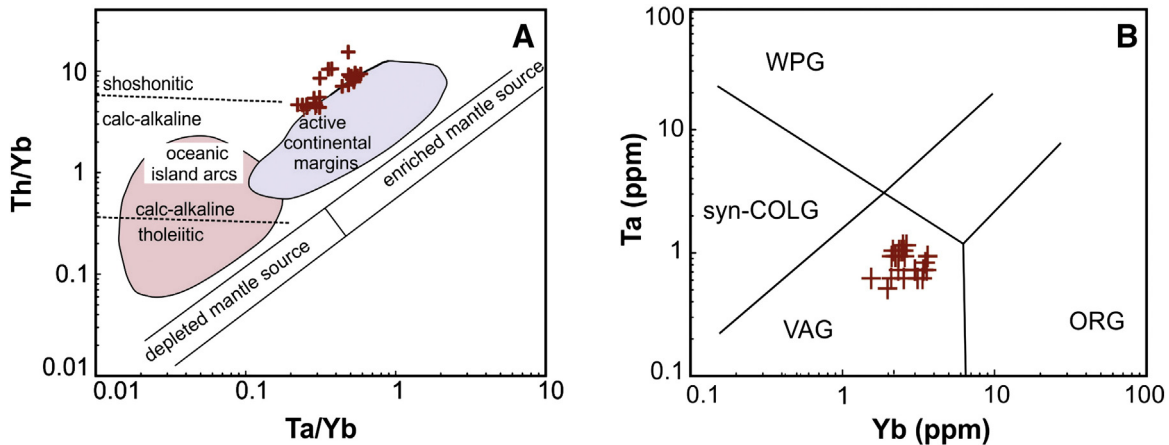


Fig. 8. Tectonic discrimination diagrams for the felsic tuffs (A: after Pearce, 1982; B: after Pearce et al., 1984).

(Eyuboglu et al., 2006). These rift-related lithological units are overlain by late Jurassic–early Cretaceous neritic carbonates formed during long-lived thermal subsidence (Fig. 11).

The second period of basin development started with break-up of the late Jurassic–early Cretaceous carbonate platform during the early Late Cretaceous. Systematic geological and geophysical studies indicate that the late Cretaceous oblique rift and/or pull-apart basins of the Eastern Pontides Orogenic Belt opened as intra-arc and back-arc basins above a south-facing subduction zone (Bektaş et al., 1995, 1999; Eyuboglu et al., 2007). These basins with different lithofacies make up different sub-belts of the Eastern Pontides Orogenic Belt from north to south, the so-called northern, southern and axial zones. Duality of the basins that were controlled by the NW, E–W and NE fault systems of the Eastern Pontides Orogenic Belt suggests an initially transtensional and subsequent transpressive regime during the late Cretaceous. While the basins have ensialic basement in the northern and southern zones, the axial zone basins are characterized by transitional or limited oceanic basement (Eyuboglu et al., 2007). This implies that diachronous drowning of the late Jurassic–early Cretaceous carbonate platform was achieved by progressive rifting (Eyuboglu et al., 2007).

The internal stratigraphy of the late Cretaceous pull-apart basins in the southern part of the Eastern Pontides Orogenic Belt is composed of two distinct lithological facies that may reflect a strike-slip cycle, from a transtensional to a transpressive tectonic regime. The lower part of the stratigraphy (opening stage) is represented by redeposited carbonate rocks that show a thinning and fining upward sequence from monogenic limestone breccia, through calcarenite, to red pelagic limestone of the late Cenonian–early Campanian (Fig. 11). The thickness and distribution of the redeposited carbonate rocks on the late Jurassic–early Cretaceous carbonate platform (Berdiga Formation) reflect the basin asymmetry in the half grabens (Fig. 11). The upper part of the stratigraphy (filling stage) is represented mainly by alternations of sandstone,

siltstone, claystone, and minor tuff, with intervening olistoliths, mainly of limestone, derived from the rift shoulders of the pull-apart basins. This upper level facies of the basins corresponds to the transpressive cycle in the pull-apart basins of the uppermost Cretaceous (Fig. 11).

It is widely accepted that there are two basic types of turbidite sequences in orogenic belts (Boggs, 1995; Einsele, 1992). Turbidites deposited from high-density flows are characterized by thick-bedded successions consisting mainly of coarse-grained sandstones and gravels. Conversely, turbidites deposited from low-density flows are represented by thin-bedded successions including lithologies consisting mainly of silt and clay-sized material. The upper part of the Kermutdere Formation, which is well distributed in the southern zone of the Eastern Pontides Orogenic Belt, consists mainly of thin to medium-bedded sandstone, siltstone, and claystone interbedded with felsic tuffs. The lithological, textural, and structural characteristics of this sequence are very similar to those of turbidites deposited from low-density flows. Although there have been a few studies on the depositional setting and geochemical characteristics of clastic lithologies within the turbiditic sequence (Eker and Korkmaz, 2011; Eren, 1983; Yilmaz, 2002), so far there hasn't been any work on their accumulation rates. In this study, the average accumulation rate for the turbiditic sequence was estimated based on zircon U–Pb ages obtained from the felsic tuff samples collected from the different levels of the sequence. U–Pb analyses of zircon grains extracted from samples KPR-3, KPR-9 and KPR-14 that were taken from the bottom, middle and upper parts of the sequence gave a weighted mean $^{206}\text{Pb}/^{238}\text{U}$ ages of 84.05 ± 0.94 (MSWD = 0.41), 81.09 ± 0.62 (MSWD = 1.16) and 77.1 ± 1.0 (MSWD = 1.2), respectively (Figs. 4 and 6). The thickness between layers of KPR-3 and KPR-9 is about 109 m, corresponding to an average accumulation rate of 36.8 cm/10 ky, between 84.05 and 81.09 Ma, without considering uncertainties in the age analyses and compaction. Thickness of the sequence between KPR-9 and KPR-14 (158 m) yields an average turbidite

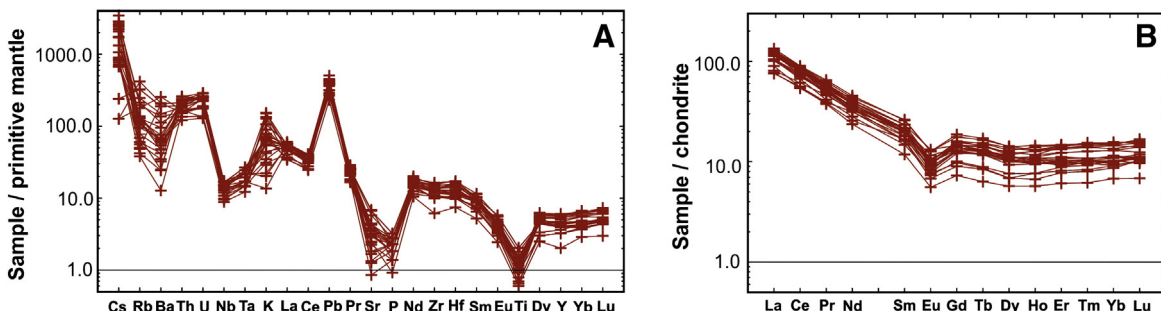


Fig. 9. Primitive mantle-normalized trace (A) and chondrite-normalized rare earth element distribution patterns (B) for the felsic tuffs (primitive mantle values: Sun and McDonough, 1989; chondrite values: Boynton, 1989).

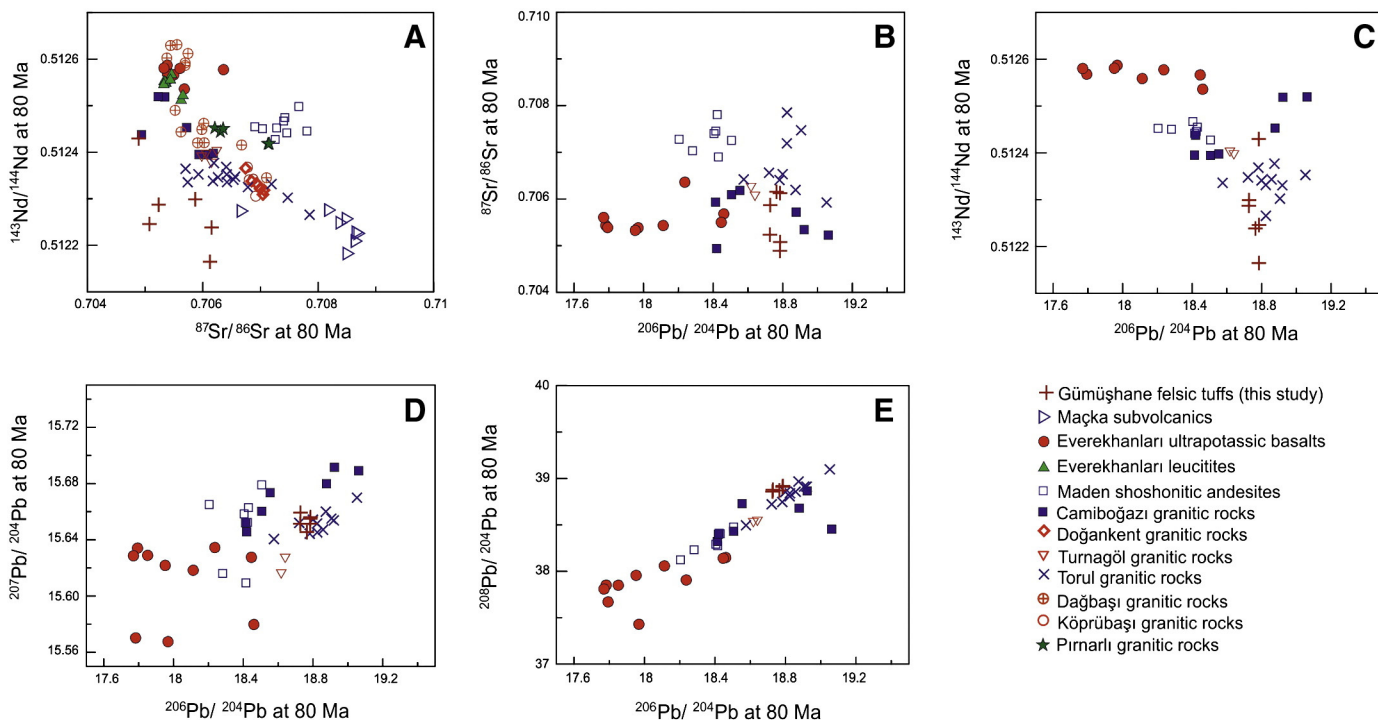


Fig. 10. Isotopic composition data from late Cretaceous sample suites exposed in the Eastern Pontides Orogenic Belt. Data include: Maçka subvolcanic rocks (Aydin, 2014), Everekhanları ultrapotassic rocks (Altherr et al., 2008 and Eyuboglu, 2010), Maden shoshonitic andesites (Eyuboglu, 2010), Camibağazı granitic rocks (Kaygusuz et al., 2014), Turnagöl granitic rocks (Kaygusuz et al., 2013), Torul granitic rocks (Kaygusuz et al., 2008), Dağbaşı granitic rocks (Kaygusuz and Aydinçakır, 2011), Köprübaşı granitic rocks (Kaygusuz and Şen, 2011), Doğankent granitic rocks (Karslı et al., 2010b) and Pınarlı granitic rocks (Karslı et al., 2012).

accumulation rate of 39.6 cm/10 ky. When considering the whole thickness of the sequence between sample KPR-3 and sample KPR-14 (267 m), the average accumulation rate of the turbiditic part of the Kermutdere Formation is about 38.4 cm/10 ky. These results indicate that the average accumulation rate of the turbiditic sequence that hosts the felsic tuffs remained constant between 36 and 40 cm/10 ky for about 7 My, implying that the overall tectonic environment was also stable over that period.

6.3. Geodynamic implications

The late Mesozoic geodynamic evolution of the Pontides Orogenic Belt, which geographically corresponds to the northern part of Anatolia and is one of the essential parts of the Alpine-Himalayan system, is still controversial due to lack of systematic geological, geophysical, geochemical and chronological data. Most authors suggest that the origin of the late Cretaceous magmatism is related to northward subduction of oceanic lithosphere (Paleotethys and/or Northern Branch of Neotethys) during the Mesozoic (Asan et al., 2014; Aydin, 2014; Dilek et al., 2010; Karslı et al., 2010a; Okay and Sahintürk, 1997; Okay et al., 1994; Şengör and Yılmaz, 1981; Topuz et al., 2005; Ustaömer and Robertson, 1996). They also suggest that this northward subduction of Tethyan oceanic lithosphere ended due to collision between the Pontide and Tauride blocks during the Paleocene; subsequent Cenozoic magmatism was generated in a post-collisional tectonic setting. However, most recent systematic geological, geophysical, geological and chronological studies indicate that the origin of the late Cretaceous magmatism cannot be explained by a northward subduction model (Eker and Korkmaz, 2011; Eyuboglu, 2010; Eyuboglu et al., 2010; Eyuboglu et al., 2011b,c,d,e,f, 2013a,b, 2014; Eyuboglu et al., 2012; Maden, 2013).

The late Cretaceous subduction-related volcanic activity started with tholeiitic-calc alkaline affinities in the Northern Zone of the Eastern

Pontides Orogenic Belt during the Turonian-Coniacian (Eyuboglu et al., 2014). This volcanic activity migrated southward over time and initiated calc-alkaline volcanism in the Southern Zone of the magmatic arc during the early Campanian, at ca. 83 Ma. The southward migration of the volcanic activity continued and passed into Campanian shoshonitic volcanism in the southernmost part of the belt at ca. 80 Ma (Eyuboglu, 2010; Eyuboglu et al., 2014). Late Cretaceous volcanic activity converted to calc alkaline-shoshonitic affinities in the north and ultrapotassic affinity in the south during Campanian-Maastrichtian time (Eyuboglu et al., 2011b, 2014). The spatial and temporal changes of late Cretaceous subduction-related arc volcanism support the existence of a south-dipping subduction zone below the Eastern Pontides magmatic arc during late Mesozoic time. Conversely, Cenozoic igneous activity started with adakitic affinity in the Axial Zone during the late Paleocene and migrated towards the north with time generating the youngest adakitic bodies along the Gumushane-Bayburt line in the Lutetian. North of this line, contemporaneous magmatism was non-adakitic and granitic, became progressively younger towards the north, and culminated in alkaline volcanism along the northern edge of the Eastern Pontides Orogenic Belt during the Neogene (Eyuboglu et al., 2011b,c). The northward migration of Cenozoic arc magmatism cannot be explained by a post-collisional setting but rather by rollback, starting in the late Paleocene (Eyuboglu et al., 2011b,c, 2014), of Tethyan oceanic lithosphere that was subducted towards the south during the late Cretaceous.

Most authors suggest that the Black Sea Basin, located north of the Eastern Pontides Orogenic Belt (Fig. 1), opened as a back-arc basin during northward subduction of the Tethyan oceanic lithosphere in the late Mesozoic (Dilek et al., 2010; Nikishin et al., 2003; Okay et al., 1994; Robertson and Dixon, 1984; Şengör and Yılmaz, 1981; Shillington et al., 2008; Ustaömer and Robertson, 1996). However, the most recent geological and geophysical studies don't support this idea (Eyuboglu et al., 2014; Maden, 2013).

Table 2
Sr-Nd-Pb isotopic data for the felsic tufts.

Sample	$^{87}\text{Rb}/^{86}\text{Sr}$	$^{87}\text{Sr}/^{86}\text{Sr}$	$^{87}\text{Sr}/^{86}\text{Sr}$ (1)	$^{147}\text{Sm}/^{144}\text{Nd}$	$^{143}\text{Nd}/^{144}\text{Nd}$	$\varepsilon\text{Nd (T)}$ (80 Ma)	$\varepsilon\text{Nd (0)}$	T_{DM} (Ga)	$^{206}\text{Pb}/^{204}\text{Pb}$	$^{206}\text{Pb}/^{204}\text{Pb}$ (1)	$^{207}\text{Pb}/^{204}\text{Pb}$	$^{208}\text{Pb}/^{204}\text{Pb}$	$^{208}\text{Pb}/^{204}\text{Pb}$ (1)
KTF-18	3.0	0.708447	0.705084	0.11101	0.512303	0.512245	-5.7	-6.5	1.19	18.785	18.645	15.649	38.919
KTF-15	2.1	0.708468	0.706128	0.1066	0.512220	0.512164	-7.2	-8.2	1.26	18.784	18.646	15.648	38.914
KTF-14	2.8	0.708096	0.704896	0.1049	0.512484	0.512429	-2.1	-3.0	0.89	18.784	18.638	15.651	38.744
KTF-11	2.7	0.709224	0.706159	0.1110	0.512296	0.512238	-5.8	-6.7	1.21	18.765	18.604	15.645	38.871
KTF-3	2.6	0.708168	0.705241	0.11249	0.512352	0.512287	-4.8	-5.6	1.29	18.727	18.620	15.651	38.728
KTF-2	2.7	0.708964	0.705876	0.1174	0.512360	0.512299	-4.6	-5.4	1.19	18.728	18.614	15.659	38.752

Heat flow studies in present-day active convergent margins indicate that the backarc and forearc basins have the mean and lowest values of heat flow, respectively, and the heat flow values increase towards land and reach the highest values at the axis of the magmatic arc (Langseth et al., 1980; Lewis et al., 1988; Stein, 2003; Uyeda, 1977; Ziagos et al., 1985). In a recent study, Maden (2013) showed by model calculations that the temperature at a depth of 100 km, and heat flow values on the Curie temperature surface, change from 706.8 °C and 14.3 mW m⁻² in the eastern Black Sea Basin to 1432.1 °C and 59.4 mW m⁻² in the Eastern Pontides arc region, supporting the existence of a south-dipping subduction zone. In convergent plate margins, the overriding plate moves towards the trench and produces a regional-scale reverse fault system that provides critical information for interpreting subduction polarity in the ancient convergent margin. The geological and geophysical studies in the Black Sea Basin indicate that the southern margin of the Black Sea Basin is bounded by a regional-scale and south-dipping reverse fault (e.g., Nikishin et al., 2003; Okay et al., 1994; Sengör and Yilmaz, 1981). Similarly, our studies reveal that the large-scale reverse fault systems in the Eastern Pontides magmatic arc, which generally formed after the late Cretaceous, are generally NE-trending and southeast-dipping (Eyuboglu et al., 2006, 2007, 2011b). The existence of south-dipping reverse fault systems in the region indicates the northward movement of the Eastern Pontides Orogenic Belt above a south-dipping subduction zone. In addition, the paleomagnetic data support the idea that the Eastern Pontides Orogenic Belt has drifted 10°–15° towards the north since the late Cretaceous (Channell et al., 1996; Van der Voo, 1968).

In recent years, the geochemical characteristics of clastic sedimentary rocks have been widely used by earth scientists who work on convergent margins and related basin development (e.g., Armstrong-Altrin and Verma, 2005; Bhatia, 1983; Eriksson et al., 1994; Floyd et al., 1991; Sun et al., 2012; Sutton and Maynard, 1993). The late Cretaceous turbidite sequence, which is one of the main subjects of this study, is well exposed in the southern part of the Eastern Pontides Orogenic Belt. However, a sequence similar in age and lithology can also be seen in a few locations in the northern part of the belt. Eker and Korkmaz (2011) suggested that the sandstones collected from sequences in the north of the arc reveal geochemical characteristics similar to those of sandstones accumulated in forearc basins with their positive Eu and negative Ce anomalies, and other trace and REE characteristics. They also emphasized that the late Cretaceous sandstones exposed in the Gumushane region indicate a back-arc basin environment with their sloped LREE and flat HREE distribution patterns, and slight negative Eu anomalies.

Finally:

- the southward migration and increasing potassium content of the late Cretaceous volcanism over time,
 - the northward migration of the Cenozoic igneous activity over time,
 - northward drift of the Eastern Pontides Orogenic Belt since the late Cretaceous,
 - the existence of a south-dipping reverse fault extending along the entire southern margin of the Black Sea Basin,
 - the existence of south-dipping large-scale reverse fault systems in the Eastern Pontides magmatic arc, and
 - heat flow values increasing from the eastern Black Sea basin towards the axis of Eastern Pontides magmatic arc
- can be best explained by a southward subduction model during the late Mesozoic–Cenozoic, rather than a northward subduction model.

6.4. Mesozoic geodynamic evolution of the Eastern Pontides Belt

Considering all of the regional geological, geophysical, geochemical and chronological data, the Mesozoic southward subduction of Tethyan oceanic lithosphere can be separated into two main stages (Eyuboglu, 2010; Eyuboglu et al., 2007). Tethyan oceanic lithosphere began rollback

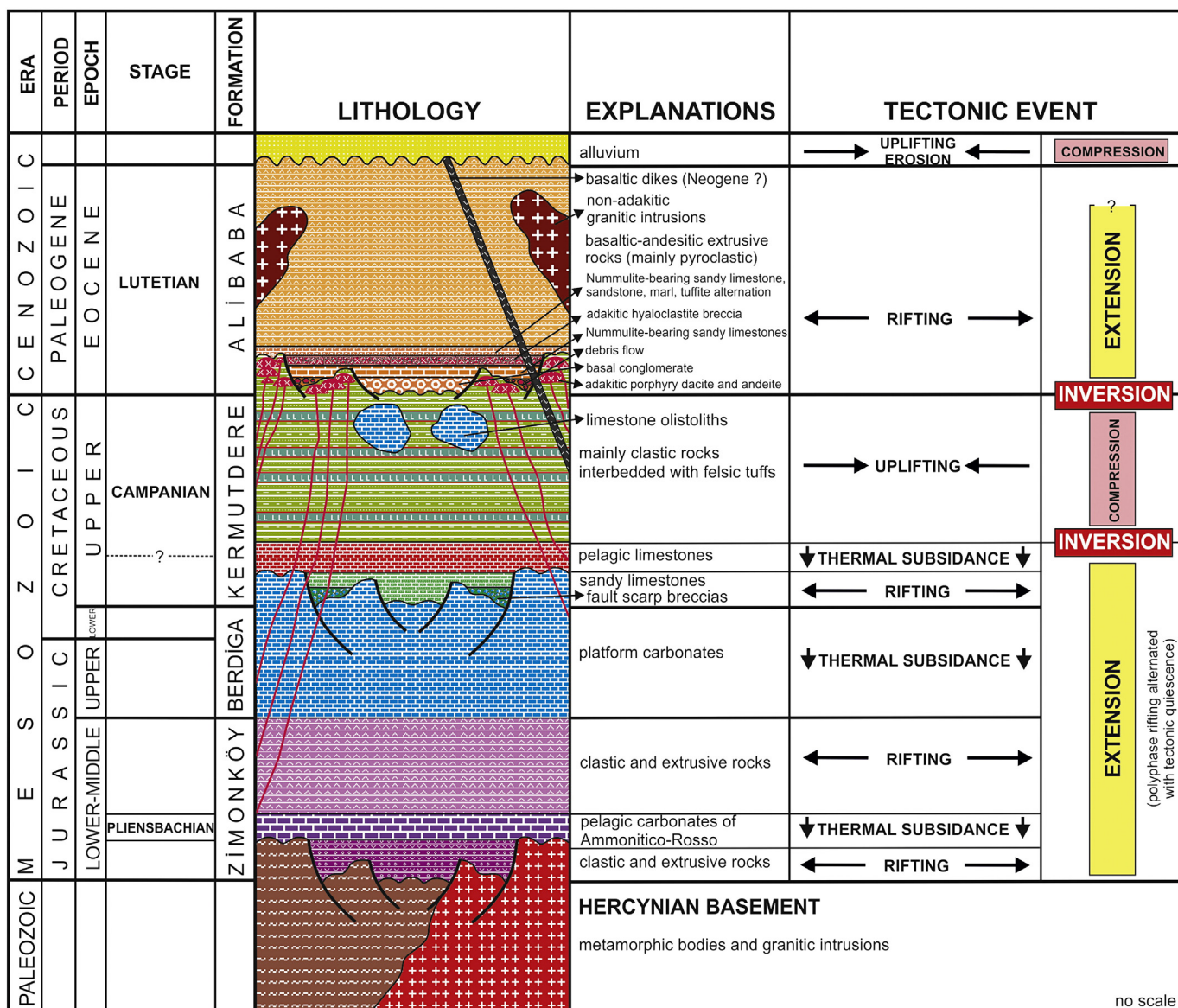


Fig. 11. Generalized stratigraphic columnar section showing the main tectonic events and lithological units of the Gümüşhane region. Modified from [Eyuboglu et al. \(2006\)](#).

during early Jurassic time. This process triggered opening of rift basins in the back-arc region of the magmatic arc and accumulated the volcano-sedimentary units in these basins (Fig. 12A). This period was followed by regional subsidence and began a tectonically and magmatically quiet period that persisted until the end of early Cretaceous (Fig. 12B). Late Jurassic–early Cretaceous platform carbonates accumulated over the early- to middle-Jurassic volcano-sedimentary units in the entire belt. During the middle Cretaceous, the first stage of Mesozoic southward subduction ended by slab breakoff of the older and denser part of the Tethyan oceanic lithosphere, which had been subducted towards the south since Paleozoic time (Fig. 12C). Slab breakoff resulted in basin development related to upwelling of asthenospheric mantle in the back-arc region of the Eastern Pontides Orogenic Belt (Fig. 12C). At this time, an ophiolitic olistostromal melange, which reflects a strike-slip cycle – from transtensional to transpressive tectonic regimes – in the deep spreading troughs of pull-apart basins (Eyuboglu et al., 2007), originally formed during the drifting stage of back-arc basin development (Neotethys ?). Resumption of southward subduction in late Cretaceous time produced intensive TH-CA magmatic activity in the northern part of the Eastern Pontides Orogenic Belt in the Turonian-Coniacian. In

addition, both intensive volcanic activity and emplacement of gabbroic and dioritic intrusions caused break-up of the carbonate platform in the northern part of the arc during early late Cretaceous time (Fig. 12D). The southward subduction of Tethyan oceanic lithosphere continued and produced calc alkaline andesitic and dacitic volcanism in the south of the arc, and high K-shoshonitic volcanism even further south during the Campanian (Fig. 12D).

7. Conclusions

The main findings of this study, which focuses on the petrogenesis and geodynamic setting of felsic tuffs interbedded with turbidites in the Southern Zone of the Eastern Pontides Orogenic Belt, are as follows:

- The abundance of felsic tuff layers in the turbidite sequence exhibits abrupt changes within short distances, as in most successions including pyroclastic lithologies, and their thickness is generally less than 2 m. These field characteristics indicate that the Kermutdere felsic tuffs are due to small-scale eruptions from local sources and are dominantly air fall, rather than ash-flow tuffs.

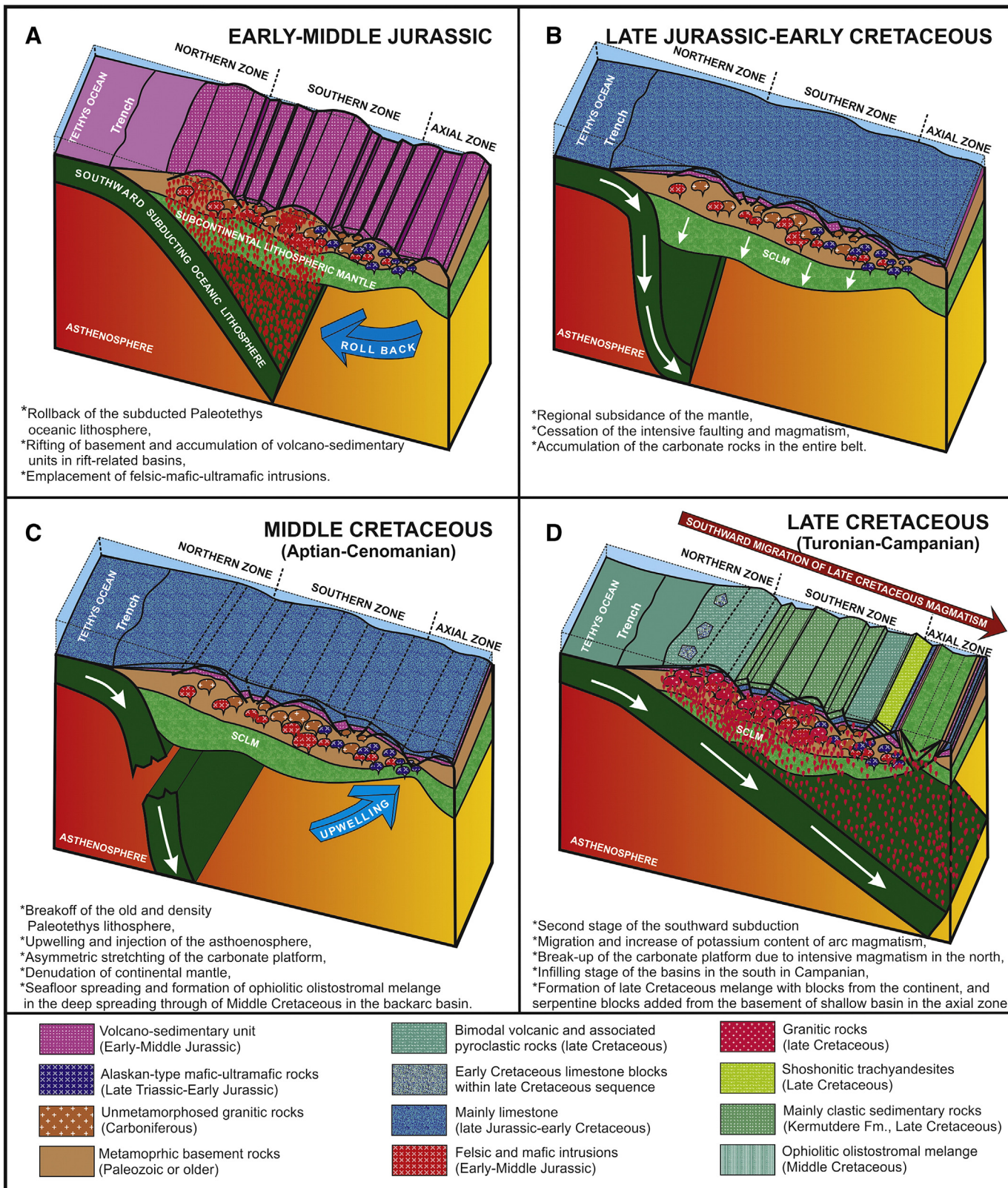


Fig. 12. Cartoon showing the Mesozoic geodynamic evolution of the Eastern Pontides Orogenic Belt.
Modified from [Eyuboglu \(2010\)](#) and [Eyuboglu et al. \(2011b, 2014\)](#).

- The tuffs, which show various degrees of alteration, can be classified as crystal-rich and crystal-poor tuffs based on petrographic data. Crystal-poor tuffs consist predominantly of 45–65% devitrified glass shards and 10–20 broken quartz crystals, whereas the crystal-rich tuffs consist of >50% crystals of various mineralogy, mostly plagioclase and quartz.
- In the type location (Kocapınar village), zircon U-Pb ages obtained from different tuff layers indicate that late Cretaceous magmatism

- began about 84 Ma ago in the Southern Zone of the Eastern Pontides Orogenic Belt (Gumushane-Kale area) and was episodically active at least through 7 Ma.
- The average accumulation rate of the turbiditic sequence hosting the Kermutdere tuffs is between 36 and 40 cm/10 ky.
 - Extensive alteration of the tuffs makes interpretation of their chemical affinity difficult. However, when compared with the other series in the Eastern Pontides Orogenic Belt, their REE distributions are consistent with either the calc-alkaline or high-K calc-alkaline series.
 - The enrichment in LIL and LRE elements relative to HFS and HRE elements, and remarkable negative Nb, Ta and Ti anomalies, suggest that they are subduction-related.
 - The remarkable similarity of the REE profiles of tuffs taken from different levels within the sequence indicates that the original source material for all tuffs was similar.
 - Considering all geological, geochemical, chronological and geophysical data, the late Mesozoic geodynamic evolution of northern Turkey can be best explained by a southward subduction model, rather than a northward subduction model.

Supplementary data to this article can be found online at <http://dx.doi.org/10.1016/j.lithos.2014.11.006>.

Acknowledgments

This study was funded by The Scientific and Technological Research Council of Turkey (TÜBİTAK Grant No: 113Y329). Special thanks are due to Dr. Francis O. Dudas for his interest, steadfast support and valuable comments. I thank Professor G. Nelson Eby (Editor-in-Chief) and two reviewers for their constructive comments, which helped us to improve the manuscript. I would also like to thank Kemal Akdag and Osman Bektaş for their contributions and helpful suggestions.

References

- Altherr, R., Topuz, G., Siebel, W., Şen, C., Meyer, H.P., Satir, M., Lahaye, Y., 2008. Geochemical and Sr–Nd–Pb isotopic characteristics of Paleocene plagioclacites from the eastern Pontides (NE Turkey). *Lithos* 105, 149–161.
- Armstrong-Altrin, J.S., Verma, S.P., 2005. Critical evaluation of six tectonic setting discrimination diagrams using geochemical data of Neogene sediments from known tectonic settings. *Sedimentary Geology* 177, 115–129.
- Arslan, M., Aliyazıcıoğlu, I., 2001. Geochemical and petrological characteristics of the Kale (Gumushane) volcanic rocks: implications for the Eocene evolution of eastern Pontide arc volcanism, Northeast Turkey. *International Geology Review* 43, 595–610.
- Arslan, M., Aslan, Z., 2006. Mineralogy, petrography and whole-rock geochemistry of the Tertiary Granitic Intrusions in the Eastern Pontides, Turkey. *Journal of Asian Earth Sciences* 27 (2), 177–193.
- Asan, K., Kurt, H., Francis, D., Morgan, G., 2014. Petrogenesis of the late Cretaceous K-rich volcanic rocks from the Central Pontide orogenic belt, North Turkey. *Island Arc* 123, 102–124.
- Aydin, F., 2014. Geochronology, geochemistry, and petrogenesis of the Maçka subvolcanic intrusions: implications for the Late Cretaceous magmatic and geodynamic evolution of the eastern part of the Sakarya Zone, northeastern Turkey. *International Geology Review*. <http://dx.doi.org/10.1080/00206814.2014.933364>.
- Bektaş, O., Van, A., Boynukalın, S., 1987. Jurassic volcanism and its geotectonic in eastern Pontides, NE Turkey. *Geological Society of Turkey Bulletin* 30, 9–19.
- Bektaş, O., Yılmaz, C., Taşlı, K., Akdağ, K., Özgür, S., 1995. Cretaceous rifting of the eastern Pontide carbonate platform (NE Turkey): the formation of carbonates breccias and turbidites as evidences of a drowned platform. *Geologia* 57 (1–2), 233–244.
- Bektaş, O., Şen, C., Atıcı, Y., Köprübaşı, N., 1999. Migration of the Upper Cretaceous subduction-related volcanism toward the back-arc basin of the eastern Pontide magmatic arc (NE Turkey). *Geological Journal* 34, 95–106.
- Bhatia, M.R., 1983. Plate tectonics and geochemical composition of sandstones. *Journal of Geology* 91 (6), 611–627.
- Boggs Jr., S., 1995. *Principles of Sedimentology and Stratigraphy*. Prentice-Hall, New Jersey (774 pp.).
- Boynton, W.V., 1984. Cosmochemistry of rare earth elements: meteorite studies. In: Henderson, P. (Ed.), *Rare Earth Element Geochemistry*. Elsevier, Amsterdam, pp. 63–114.
- Boynukalın, S., 1991. Dereli (Giresun) baraj yeri ve göl alanının mühendislik jeolojisi ve çevre kayalarının jeomekanik özellikleri. Unpublished PhD Thesis KTU Fen Bilimleri Enstitüsü, Trabzon 255p.
- Channell, J.E.T., Tüysüz, O., Bektaş, O., Şengör, A.M.C., 1996. Jurassic–Cretaceous paleomagnetism and paleogeography of the Pontides (Turkey). *Tectonics* 15, 201–212.
- Dilek, Y., Imamverdiyev, N., Altunkaynak, Ş., 2010. Geochemistry and tectonics of Cenozoic volcanism in the Lesser Caucasus (Azerbaijan) and the peri-Arabian region: collision-induced mantle dynamics and its magmatic fingerprint. *International Geology Review* 52 (4–6), 536–578.
- Dokuz, A., 2011. A slab detachment and delamination model for the generation of Carboniferous high-potassium I-type magmatism in the Eastern Pontides, NE Turkey: the Kose composite pluton. *Gondwana Research* 19 (4), 926–944.
- Einsele, G., 1992. *Sedimentary Basins: Evolution, Facies, and Sediment Budget*. Springer-Verlag, Heidelberg (628 pp.).
- Eker, C.S., Korkmaz, S., 2011. Mineralogy and whole rock geochemistry of late Cretaceous sandstones from the eastern Pontides (NE Turkey). *Neues Jahrbuch für Mineralogie* 188 (3), 235–256.
- Eren, M., 1983. *Gümüşhane-Kale arasındaki jeoloji ve mikrofaziyesi* (Msc Thesis) Karadeniz Üniversitesi Fen Bilimleri Enstitüsü, (197 pp.).
- Eriksson, P.G., Schreiber, U.M., Reczko, B.F.F., Snyman, C.P., 1994. Petrography and geochemistry of sandstones interbedded with the Roonberg Felsite Group (Transvaal Sequence, South Africa): implications for provenance and tectonic setting. *Journal of Sedimentary Research* 64A (4), 836–846.
- Eyuboglu, Y., 2010. Late Cretaceous high-K volcanism in the Eastern Pontide Orogenic Belt, and its implications for the geodynamic evolution of NE Turkey. *International Geology Review* 52 (2–3), 142–186.
- Eyuboglu, Y., Bektaş, O., Seren, A., Maden, N., Jacoby, W.R., Özer, R., 2006. Three axial extensional deformation and formation of the Liassic rift basins in the Eastern Pontides (NE Turkey). *Geologica Carpathica* 57 (5), 337–346.
- Eyuboglu, Y., Bektaş, O., Pül, D., 2007. Mid-Cretaceous olistostromal ophiolitic melange developed in the back-arc basin of the eastern Pontide magmatic arc (NE Turkey). *International Geology Review* 49 (12), 1103–1126.
- Eyuboglu, Y., Dilek, Y., Bozkurt, E., Bektaş, O., Rojay, B., Şen, C., 2010. Geochemistry and geochronology of a reversely-zoned, Alaskan-type ultramafic–mafic complex in the Eastern Pontides, NE Turkey. In: Santosh, M., Maruyama, S. (Eds.), *A tribute to Akiko Miyashiro*. *Gondwana Research* 18, pp. 230–252.
- Eyuboglu, Y., Santosh, M., Bektaş, O., Chung, S.L., 2011a. Late Triassic subduction-related ultramafic–mafic magmatism in the Amasya area (Eastern Pontides, NE Turkey): implications for the ophiolite conundrum in eastern Mediterranean. *Journal of Asian Earth Sciences* 42 (3), 234–257.
- Eyuboglu, Y., Chung, S.L., Dudas, F.O., Santosh, M., Akaryali, E., 2011b. Transition from shoshonitic to adakitic magmatism in the Eastern Pontides, NE Turkey: implications for slab window melting. *Gondwana Research* 19, 413–429.
- Eyuboglu, Y., Santosh, M., Dudas, F.O., Chung, S.L., Akaryali, E., 2011c. Migrating magmatism in a continental arc: geodynamics of the Eastern Mediterranean revisited. *Journal of Geodynamics* 52, 2–15.
- Eyuboglu, Y., Santosh, M., Chung, S.L., 2011d. Crystal fractionation of adakitic magmas in the crust–mantle transition zone: petrology, geochemistry and U–Pb zircon chronology of the Seme adakites, Eastern Pontides, NE Turkey. *Lithos* 121, 151–166.
- Eyuboglu, Y., Santosh, M., Chung, S.L., 2011e. Petrochemistry and U–Pb ages of adakitic intrusions from the Pulur massif (Eastern Pontides, NE Turkey): implications for slab roll-back and ridge subduction associated with Cenozoic convergent tectonics in eastern Mediterranean. *Journal of Geology* 119, 394–417.
- Eyuboglu, Y., Santosh, M., Bektaş, O., Ayhan, S., 2011f. Arc magmatism as a window to plate kinematics and subduction polarity: example from the Eastern Pontides belt, NE Turkey. *Geoscience Frontiers* 2 (1), 49–56.
- Eyuboglu, Y., Santosh, M., Yi, K., Bektaş, O., Kwon, S., 2012. Discovery of Miocene adakitic dacite from the Eastern Pontides Belt and revised geodynamic model for the late Cenozoic Evolution of eastern Mediterranean region. *Lithos* 146–147, 218–232.
- Eyuboglu, Y., Santosh, M., Dudas, F.O., Akaryali, E., Chung, S.L., Akdag, K., Bektaş, O., 2013a. The nature of transition from adakitic to non-adakitic magmatism in a slab–window setting: a synthesis from the eastern Pontides, NE Turkey. *Geoscience Frontiers* 4, 353–375.
- Eyuboglu, Y., Dudas, F.O., Santosh, M., Yi, K., Kwon, S., Akaryali, E., 2013b. Petrogenesis and U–Pb zircon chronology of adakitic porphyries within the Kop ultramafic massif (Eastern Pontides Orogenic Belt, NE Turkey). *Gondwana Research* 24, 742–766.
- Eyuboglu, Y., Santosh, M., Yi, K., Tüysüz, N., Korkmaz, S., Akaryali, E., Dudas, F., Bektaş, O., 2014. The Eastern Black Sea-type volcanogenic massive sulfide deposits: geochemistry, zircon U–Pb geochronology and an overview of the geodynamics of ore genesis. *Ore Geology Reviews* 59, 29–54.
- Floyd, P.A., Shail, R., Leveridge, B.E., Franke, W., 1991. Geochemistry and provenance of Rhenohercynian synorogenic sandstones: implications for tectonic environment discrimination. *Geological Society, London, Special Publications* 57, 173–188.
- Gill, J.B., 1981. *Orogenic Andesites and Plate Tectonics*. Springer-Verlag, Berlin Heidelberg New York (390 pp.).
- Hastie, A.R., Kerr, A.C., Pearce, J.A., Mitchell, S.F., 2007. Classification of altered volcanic island arc rocks using immobile trace elements: development of the Th–Co discrimination diagram. *Journal of Petrology* 48 (12), 2341–2357.
- Hawkesworth, C.J., Herdt, J.M., McDermott, F., Ellam, R.M., 1991. Destructive margin magmatism and the contributions from the mantle wedge and subducted crust. *Australian Journal of Earth Sciences* 38, 577–594.
- Karslı, O., Dokuz, A., Uysal, İ., Aydin, F., Kandemir, R., Wijbrans, R.J., 2010a. Generation of the early Cenozoic adakitic volcanism by partial melting of mafic lower crust, Eastern Turkey: implications for crustal thickening to delamination. *Lithos* 114, 109–120.
- Karslı, O., Dokuz, A., Uysal, İ., Aydin, F., Chen, B., Kandemir, R., Wijbrans, R.J., 2010b. Relative contributions of crust and mantle to generation of Campanian high-K calc-alkaline I-type granitoids in a subduction setting, with special reference to the Harsit pluton, eastern Turkey. *Contributions to Mineralogy and Petrology* 160, 467–487.

- Karslı, O., Caran, Ş., Dokuz, A., Çoban, H., Chen, Bin, Kandemir, R., 2012. A-type granitoids from the Eastern Pontides, NE Turkey: records for generation of hybrid A-type rocks in a subduction-related environment. *Tectonophysics* 530–531, 208–224.
- Kaygusuz, A., Aydinçakır, E., 2011. Petrogenesis of a Late Cretaceous composite pluton from the eastern Pontides: the Dagbasi pluton, NE Turkey. *Neues Jahrbuch Fur Mineralogie-Abhandlungen* 188, 211–233.
- Kaygusuz, A., Şen, C., 2011. Calc-alkaline I-type plutons in the eastern Pontides, NE Turkey: U–Pb zircon ages, geochemical and Sr–Nd isotopic compositions. *Chemie der Erde* 71, 59–75.
- Kaygusuz, A., Siebel, W., Sen, C., Satır, M., 2008. Petrochemistry and petrology of I-type granitoids in an arc setting: the composite Torul pluton, eastern Pontides, NE Turkey. *International Journal of Earth Sciences* 97, 739–764.
- Kaygusuz, A., Chen, B., Aslan, Z., Siebel, W., Sen, C., 2009. U–Pb SHRIMP zircon ages, geochemical and Sr–Nd isotopic compositions of the Late Cretaceous I-type Sariosman Pluton, Eastern Pontides, NE Turkey. *Turkish Journal of Earth Sciences* 18 (4), 549–581.
- Kaygusuz, A., Arslan, M., Siebel, W., Şen, C., 2011. Geochemical and Sr–Nd isotopic characteristics of post-collisional calc-alkaline volcanics in the Eastern Pontides (NE Turkey). *Turkish Journal of Earth Sciences* 20 (1), 137–159.
- Kaygusuz, A., Arslan, M., Siebel, W., Sipahi, F., İlbeli, N., 2012. Geochronological evidence and tectonic significance of Carboniferous magmatism in the southwest Trabzon area, eastern Pontides, Turkey. *International Geology Review* 54 (15), 1776–1800.
- Kaygusuz, A., Sipahi, F., İlbeli, N., Arslan, M., Chen, B., Aydinçakır, E., 2013. Petrogenesis of the late Cretaceous Turnagöl intrusion in the eastern Pontides: implications for magma genesis in the arc setting. *Geoscience Frontiers* 4 (4), 423–438.
- Kaygusuz, A., Arslan, M., Siebel, W., Sipahi, F., İlbeli, N., Temizel, I., 2014. LA-ICP MS zircon dating, whole-rock and Sr–Nd–Pb–O isotope geochemistry of the Camıboğazı pluton, Eastern Pontides, NE Turkey: implications for lithospheric mantle and lower crustal sources in arc-related I-type magmatism. *Lithos* 192–195, 271–290.
- Langseth, M.G., Hobart, M.A., Horai, K., 1980. Heat flow in the Bering Sea. *Journal of Geophysical Research* 85, 3740–3750.
- LeBas, M.J., Lemaître, R.W., Streckeisen, A., Zanettin, B., 1986. A chemical classification of volcanic-rocks based on the total alkali silica diagram. *Journal of Petrology* 27 (3), 745–750.
- Lewis, T.J., Bentkowski, W.H., Davis, E.E., Hyndman, R.D., Souther, J.G., Wright, J.A., 1988. Subduction of the Juan de Fuca plate: thermal consequences. *Journal of Geophysical Research* 93, 15207–15225.
- Maden, N., 2013. Geothermal structure of the eastern Black Sea basin and the Eastern Pontides Orogenic Belt: implications for subduction polarity of Tethys oceanic lithosphere. *Geoscience Frontiers* 4, 389–398.
- Murphy, J.B., 2007. Arc magmatism II: geo-chemical and isotopic characteristics. *Journal of the Geological Association of Canada* 34, 1–38.
- Nikishin, A.M., Korotaev, M.V., Ershov, A., Brunet, M.F., 2003. The Black Sea basin: tectonic history and Neogene–Quaternary rapid subsidence modelling. *Sedimentary Geology* 156, 149–168.
- Okay, A.I., Sahintürk, Ö., 1997. Geology of the Eastern Pontides. In: Robinson, A.G. (Ed.), *Regional and Petroleum Geology of the Black Sea and Surrounding Region*. American Association of Petroleum Geologists Memoir 68, pp. 291–311.
- Okay, A.I., Şengör, A.M.C., Görür, N., 1994. Kinematic history of the opening of the Black Sea and its effect on the surrounding regions. *Geology* 22, 267–270.
- Pearce, J.A., 1982. Trace element characteristics of lavas from destructive plate boundaries. In: Thorpe, R.S. (Ed.), *Orogenic Andesites and Related Rocks*. John Wiley and Sons, Chichester, England, pp. 528–548.
- Pearce, J.A., Harris, N.B.W., Tindle, A.G., 1984. Trace element discrimination diagrams for the tectonic interpretation of granitic rocks. *Journal of Petrology* 25, 956–983.
- Rickwood, P.C., 1989. Boundary lines within petrologic diagrams which use oxides of major and minor elements. *Lithos* 22, 247–263.
- Ringwood, A.E., 1990. Slab–mantle interactions: 3. Petrogenesis of intraplate magmas and structure of the upper mantle. *Chemical Geology* 82, 187–207.
- Robertson, A.H.F., Dixon, J.E., 1984. Introduction: aspects of the geological evolution of the eastern Mediterranean. In: Dixon, J.E., Robertson, A.H.F. (Eds.), *The Geological Evolution of the Eastern Mediterranean*. Geological Society of London Special Publication 17, pp. 1–74.
- Rubatto, D., 2002. Zircon trace element geochemistry: partitioning with garnet and the link between U–Pb ages and metamorphism. *Chemical Geology* 184, 123–138.
- Şen, C., 2007. Jurassic volcanism in the Eastern Pontides: is it rift related or subduction related? *Turkish Journal of Earth Sciences* 16, 523–539.
- Şengör, A.M.C., Yılmaz, Y., 1981. Tethyan evolution of Turkey: a plate tectonic approach. *Tectonophysics* 75, 181–241.
- Shillington, D.J., White, N., Minshull, T.A., Edwards, G.R.H., Jones, S.M., Edwards, R.A., Scott, C.L., 2008. Cenozoic evolution of the eastern Black Sea: a test of depth-dependent stretching models. *Earth and Planetary Science Letters* 265, 360–378.
- Stein, C.A., 2003. Heat flow and flexure at subduction zones. *Geophysical Research Letters* 30 (23). <http://dx.doi.org/10.1029/2003GL018478>.
- Sun, S.S., McDonough, W.F., 1989. Chemical and isotopic systematic of ocean basalts: implications for mantle composition and process. In: Saunders, A.D., Norry, M.J. (Eds.), *Magmatism in the Ocean Basins*. Geological Society of London 42, pp. 313–345.
- Sun, L., Gui, H., Chen, S., 2012. Geochemistry of sandstones from the Neoproterozoic Shijia Formation, northern Anhui Province, China: implications for provenance, weathering and tectonic setting. *Chemie der Erde-Geochemistry* 72 (3), 253–260.
- Sutton, S.J., Maynard, J.B., 1993. Petrology, mineralogy, and geochemistry of sandstones of the lower Huronian Matinenda Formation: resemblance to underlying basement rocks. *Canadian Journal of Earth Sciences* 30 (6), 1209–1223.
- Topuz, G., Altherr, R., Schwarz, W.H., Siebel, W., Satır, M., Dokuz, A., 2005. Post-collisional plutonism with adakite-like signatures: the Eocene Sarayçıl granodiorite (Eastern Pontides, Turkey). *Contributions to Mineralogy and Petrology* 150, 441–455.
- Topuz, G., Altherr, R., Schwarz, W.H., Dokuz, A., Meyer, H.P., 2007. Variscan amphibolite-facies rocks from the Kurtoglu metamorphic complex (Gumüşhane area, Eastern Pontides, Turkey). *International Journal of Earth Sciences* 96 (5), 861–873.
- Topuz, G., Altherr, R., Siebel, W., Schwarz, W.H., Zack, T., Hasozbek, A., Barth, M., Satır, M., Sen, C., 2010. Carboniferous high-potassium I-type granitoid magmatism in the Eastern Pontides: the Gumüşhane pluton (NE Turkey). *Lithos* 116 (1–2), 92–110.
- Ustaömer, T., Robertson, A.H.F., 1996. Paleotethyan tectonic evolution of the North Tethyan margin in the central Pontides, N Turkey. In: Erler, A., Ercan, T., Bingöl, E., Ören, S. (Eds.), *International Symposium on the Geology of the Black Sea Region, Proceedings—I*, pp. 24–33.
- Uyeda, S., 1977. Some basic problems in the trench–arc–back arc system, in Island Arcs. In: Talwani, M., Pitman III, W.C. (Eds.), *Deep-sea Trenches and Back-arc Basins*, Maurice Ewing Ser 1. AGU, Washington, D.C., pp. 1–14.
- Van der Voo, R., 1968. Jurassic, Cretaceous and Eocene pole positions from northeastern Turkey. *Tectonophysics* 6 (3), 251–269.
- Williams, I.S., 1998. U–Th–Pb geochronology by ion microprobe. In: McKibben, M.A., Shanks, W.C., Ridley, W.I. (Eds.), *Applications of Microanalytical Techniques to Understanding Mineralizing ProcessesReviews in Economic Geology* 7. Society of Economic Geologists, pp. 1–35.
- Winchester, J.A., Floyd, P.A., 1977. Geochemical discrimination of different magma series and their differentiation products using immobile elements. *Chemical Geology* 20, 325–343.
- Yılmaz, C., 2002. Tectono-sedimentary records and controlling factors of the Mesozoic sedimentary basins in the Gümüşhane-Bayburt region. *Geological Bulletin of Turkey* 45 (1), 141–164.
- Ziagos, J.P., Blackwell, D.D., Mooser, F., 1985. Heat flow in southern Mexico and the thermal effects of subduction. *Journal of Geophysical Research* 90, 5410–5420.